

## Crustal and uppermost mantle structure of the Bohemian Massif based on CELEBRATION 2000 data

P. Hrubcová,<sup>1</sup> P. Šroda,<sup>2</sup> A. Špičák,<sup>1</sup> A. Guterch,<sup>2</sup> M. Grad,<sup>3</sup> G. R. Keller,<sup>4</sup> E. Brueckl,<sup>5</sup> and H. Thybo<sup>6</sup>

Received 11 March 2004; revised 20 October 2004; accepted 17 May 2005; published 10 November 2005.

[1] The deep structure of the Bohemian Massif (BM), the largest stable outcrop of Variscan rocks in central Europe, was studied using the data of the international seismic refraction experiment Central European Lithospheric Experiment Based on Refraction (CELEBRATION) 2000. The data were interpreted by seismic tomographic inversion and by two-dimensional (2-D) trial-and-error forward modeling of  $P$  and  $S$  waves. Additional constraint on crustal structure was given by amplitude modeling using the reflectivity method and gravity modeling. Though consolidated, the BM can be subdivided into several tectonic units separated by faults, shear zones, or thrusts reflecting varying influence of the Cadomian and Variscan orogeneses: the Saxothuringian, Barrandian, Moldanubian, and Moravian. Velocity models determine three types of crust-mantle transition in the BM reflecting variable crustal thickness and delimiting contacts of tectonic units in depth. The NW area, the Saxothuringian, has a highly reflective lower crustal layer above Moho with a strong velocity contrast at the top of this layer. This reflective laminated lower crust reaches depths of 26–35 km and is characteristic for the Saxothuringian unit, which was subject to eastward subduction. The Moldanubian in the central part is characterized by the deepest (39 km) and the most pronounced Moho within the whole BM with a strong velocity contrast  $6.9\text{--}8.1\text{ km s}^{-1}$ . A thick crust-mantle transition zone in the SE, with velocity increase from  $6.8$  to  $7.8\text{ km s}^{-1}$  over the depth range of 23–40 km, seems to be the characteristic feature of the Moravian overthrust by the Moldanubian during Variscan collision.

**Citation:** Hrubcová, P., P. Šroda, A. Špičák, A. Guterch, M. Grad, G. R. Keller, E. Brueckl, and H. Thybo (2005), Crustal and uppermost mantle structure of the Bohemian Massif based on CELEBRATION 2000 data, *J. Geophys. Res.*, *110*, B11305, doi:10.1029/2004JB003080.

### 1. Introduction

[2] The Bohemian Massif is a large complex terrain consolidated in the Paleozoic, located on the territory of the Czech Republic, partly Germany, Poland, and Austria. It forms the easternmost rim of the Variscan belt, a Paleozoic chain extending from southern Iberia to the Bohemian Massif in central Europe. Its configuration is the result of convergence and collision between two main continents, Laurentia-Baltica-Avalonia and Gondwana, after the closure of various oceanic basins, followed by obduction, continental collision, continental subduction, and strike-slip faulting between 500 and 250 Ma. While the postcollisional history

of the Variscan Bohemian Massif is relatively clear, the kinematics of plate movements before and during collision is still subject of debates.

[3] The fan-like shape of the Variscan belt mainly in the east European part shows that the key mechanism of its evolution was two-sided lithospheric subduction [Matte, 1991]. This subduction was accompanied by crustal stacking and thickening mainly at the crust-mantle boundary with production of various granitoids by melting of the middle and lower parts of the crust. Also, Meissner and Wever [1986], studying the deep structure of the European Variscan crust showed that the pre-Permian thrusts outcropping at the surface are rooted in the lower crust, at Moho, or in the mantle. Thus the Bohemian Massif as a stable exposure of pre-Permian rocks offers the evidences of the Variscan tectonic development. Studying the deep structure of the Bohemian Massif can bring the verification of the subduction-collision processes and better delineation of subduction zones with depth.

[4] In our paper, we present the crustal and uppermost mantle structure in different parts of the Bohemian Massif based on the interpretation of seismic data along the refraction and wide-angle reflection profile CEL09 of the Central European Lithospheric Experiment Based on

<sup>1</sup>Geophysical Institute, Academy of Sciences of the Czech Republic, Prague, Czech Republic.

<sup>2</sup>Institute of Geophysics, Polish Academy of Sciences, Warsaw, Poland.

<sup>3</sup>Institute of Geophysics, University of Warsaw, Warsaw, Poland.

<sup>4</sup>Department of Geological Sciences, University of Texas at El Paso, El Paso, Texas, USA.

<sup>5</sup>Vienna University of Technology, Vienna, Austria.

<sup>6</sup>Geological Institute, University of Copenhagen, Copenhagen, Denmark.

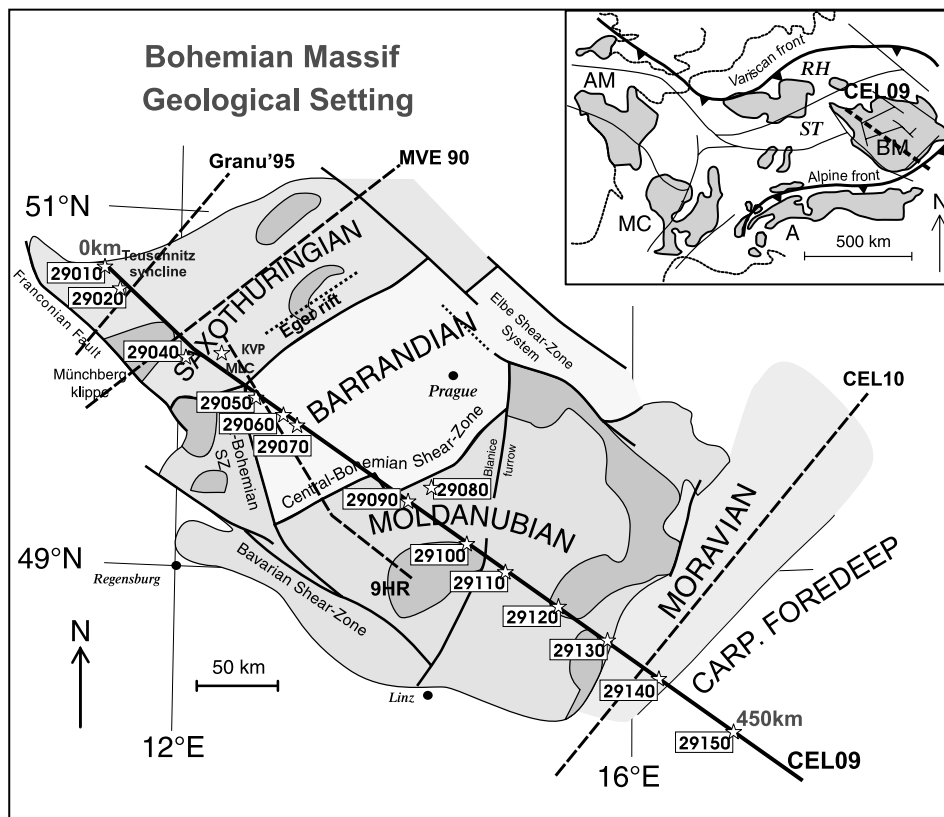


**Figure 1.** Major tectonic units of the Bohemian Massif and its setting within the European Variscides with the CELEBRATION 2000 CEL09 line. BM, Bohemian Massif; AM, Armorican Massif; MC, Massif Central; A, Alps; ST, Saxothuringian Zone; RH, Rhenohercynian Zone [after Pitra *et al.*, 1999; Franke *et al.*, 2000]. MLC, Mariánské Lázně Complex; KVP, Karlovy Vary Pluton. Stars mark positions of the individual shot points along the profile. Intersections with other seismic refraction and reflection experiments (Granu'95, MVE 90, 9HR, CEL10) are marked.

Refraction (CELEBRATION) 2000 experiment [Guterch *et al.*, 2003]. This profile traverses the whole Bohemian Massif in NW-SE direction and in the SE it continues to the west Carpathians (Figure 1). For the interpretation we chose the tomographic inversion routine of Hole [1992] as a tool to determine the preliminary seismic  $P$  wave velocity distribution in the crust using first arrivals. The resulting tomographic model was further improved by two-dimensional (2-D) trial-and-error forward modeling using a ray-tracing algorithm [Červený and Pšenčík, 1984] for  $P$  and  $S$  refracted and reflected waves. The differences in the properties of individual crustal blocks of the Bohemian Massif were further studied by modeling of the seismic wave field with the reflectivity method [Fuchs and Müller, 1971]. Gravity modeling complemented the velocity analysis. In this study we concentrate on velocity variations along the profile; azimuthal anisotropic studies are a matter of other investigations [e.g., Růžek *et al.*, 2003; Vavryčuk *et al.*, 2004; Plomerová *et al.*, 1984].

[5] So far, the Bohemian Massif has been studied mainly to show the depth of the Moho discontinuity. New insight into the deep structure of the Bohemian Massif can help to complement this knowledge, determine the crustal thickness and show the differences in crustal and upper mantle

structures in three areas pertaining to different Paleozoic regimes. Contrasts in seismic properties reflect compositional variances resulting from crust-forming processes during the Paleozoic tectonic development.

## 2. Geology and Tectonic Evolution of the Region

[6] The Bohemian Massif is one of the largest stable outcrops of pre-Permian rocks in central and western Europe. It forms the easternmost part of the Variscan Belt, which developed approximately between 500 and 250 Ma during a period of large-scale crustal convergence, collision of continental plates and microplates and subduction [Matte *et al.*, 1990]. It consists mainly of low- to high-grade metamorphic and plutonic Paleozoic rocks. On the basis of the respective effects of the Cadomian and Variscan orogenesis, the area of the Bohemian Massif can be subdivided into several tectonostratigraphic units, the Saxothuringian, Barrandian, Moldanubian and Moravian, separated by faults, shear zones or thrusts (see Figure 1).

[7] The Moldanubian unit represents a major crystalline segment within the Bohemian Massif and its boundary with the Saxothuringian in the NW is regarded to be a suture-type discontinuity. A structurally higher unit, the Barrandian, has been thrust over the Saxothuringian rocks toward

the northwest, while in the SE it has been thrust in southerly direction over the Moldanubian. It is separated from the latter by a major NE-SW trending Variscan dextral fault, the Central Bohemian Shear Zone (CBSZ), obscured by the intrusion of the Central Bohemian Pluton [Dallmeyer *et al.*, 1994]. The Moldanubian/Moravian boundary in the east has the character of a ductile shear zone with significant translation of the Moldanubian over the Moravian unit. According to Finger and Steyrer [1995], Moldanubian overthrust was the final stage of the subduction of the oceanic crust and subsequent Variscan collision between Moldanubian and Moravian units. The Moravian unit consists of a Cadomian basement overlain by the Moravicum and Silesicum nappes and to the east it submerges beneath the Carpathian Foredeep, where it forms the basement reactivated during the Alpine orogeny.

[8] The mafic Mariánské Lázně Complex (MLC), situated between the Saxothuringian and Barrandian, represents an important suture comprising segments of oceanic crust, which were subducted and metamorphosed during the Variscan orogeny and later thrust over the SE margin of the Saxothuringian [Vrána *et al.*, 1997]. This complex probably represents a boundary between two different Variscan tectonic regimes and a zone, which was reactivated later by younger tectonic movements [Babuška and Plomerová, 2000]. In the NE it adjoins the intrusion of the granitoid Karlovy Vary Pluton (KVP).

[9] From a tectonic point of view, one of the major deformation events occurred during the Variscan orogeny. Then the Bohemian Massif was sandwiched between high-grade Variscan metamorphic areas, represented by two opposing subduction zones, at first of an oceanic, then of a continental character [Matte, 2001]. The oldest deformational structures occur in the Barrandian and are associated with the earliest stages of the Saxothuringian eastward subduction and shortening of the plate. The upper plate developed into a lithospheric-scale arc system, which was manifested by the intrusion of the Central Bohemian Pluton, steeply dipping to the east along the eastern boundary of the Barrandian [Schulmann *et al.*, 2002].

### 3. Previous Geophysical Studies in the Area

[10] The beginning of the investigation of the Bohemian Massif and its deep structure is associated with the deep seismic sounding profiles recorded on the territory of the Czech Republic as a part of the international "Upper Mantle Project" [Beránek and Zouňková, 1977]. The interpretation of these refraction measurements indicated the position of the Moho discontinuity with a maximum depth of 39 km in the central part of the Bohemian Massif and a less pronounced Moho at a depth of about 32 km at the eastern edge of the Bohemian Massif [Beránek and Zátoupek, 1981].

[11] Later, these measurements were complemented by reflection profiling, as well as by other geophysical methods [see, e.g., Bucha and Bližkovský, 1994]. The deep seismic reflection profile 9HR extending from SE Germany to southern Bohemia (Figure 1) showed a crustal thickness increasing from 31 km in the NW to 39 km in the south. Combined seismic and gravity interpretation [Tomek *et al.*, 1997; Švancara and Chlupáčová, 1997] delimited the thickness of granitoid plutons and mafic intrusions, and

showed overthrusting along a SE dipping contact zone in western Bohemia.

[12] The most recent research has been done in the NW of the Bohemian Massif, in Germany. There, the seismic refraction and wide-angle reflection profile GRANU'95 [Enderle *et al.*, 1998] and deep reflection profile MVE 90 as part of the DEKORP investigation [DEKORP Research Group, 1994] showed the velocity structure of the Saxothuringian belt in SE Germany, where laminated lower crust was indicated by MVE 90 data.

[13] Continuous monitoring of seismic activity in the western part of the Bohemian Massif shows frequent occurrence of intraplate earthquake swarms with magnitudes up to 4.5. According to Horálek *et al.* [1996] and Fischer and Horálek [2003], the hypocenters of these earthquake swarms are located in the upper and middle crust down to about 20 km depth with the majority between 5 and 15 km. This seismic area, also characteristic of numerous mineral springs and CO<sub>2</sub> emissions, encompasses the western termination of the Eger Rift (see Figure 1), a geodynamically active zone of the European Cenozoic Rift System [Prodehl *et al.*, 1995].

### 4. Data Acquisition and Processing

[14] The deep structure of the Bohemian Massif was studied along the refraction and wide-angle reflection profile CEL09 using the data of the international seismic refraction experiment Central Europe Lithospheric Experiment Based on Refraction 2000 (CELEBRATION) [Guterch *et al.*, 2003]. The NW-SE oriented profile CEL09 starts in the Saxothuringian in the NW, intersects the Mariánské Lázně amphibolite complex and continues to the Barrandian. Then it crosses the granitoid intrusions spreading along the Central Bohemian Shear Zone and continues to the Moldanubian and Moravian. Farther to the SE, it continues across the Vienna Basin into the Carpathians. The interpreted part of the profile in this paper is 450 km long and ends at the contact of the Bohemian Massif with the Carpathian Foredeep (Figure 1).

[15] Along the interpreted part of the profile, 20 shots were fired, with charges ranging from 210 kg to 10 000 kg of explosives. Some of the shots (5 in all) were shot twice and the recordings were stacked in order to improve the signal-to-noise ratio. The average distance between the shots was 30 km with a station spacing of 2.7 km. The positions of the shot points and stations were measured by GPS; the origin time was controlled by a DCF77 timer with an accuracy of 3 ms [see also Málek *et al.*, 2001]. For more details on the geometry of the experiment refer to Guterch *et al.* [2003] and Růžek *et al.* [2003].

[16] Refraction and wide-angle reflection data were sampled at intervals of 10 ms and were recorded mainly by one-component stations REFTEK-125 (TEXAN), complemented by three-component REFTEK and PDAS stations. The station sensors were 4.5 Hz geophones. Data processing included shot time corrections and band-pass filtering of the whole data set (usually 2–15 Hz) in order to remove low- and high-frequency noise. The frequency content of the seismic data was highly variable for different shot points, probably due to the varying local environment and due to different shooting techniques (drill hole shots,

quarry blasts). Thus the filter window was determined interactively during data interpretation, depending on the data quality and the frequency content. Recordings were sorted into shot gathers; seismic sections were trace normalized to the maximum amplitude along the trace and plotted with a reduction velocity of  $8 \text{ km s}^{-1}$ .

## 5. Seismic Wave Field

[17] Refraction and wide-angle reflection data used for the interpretation allow several seismic  $P$  wave phases to be correlated (see Figures 2–4). In the first arrivals, we can distinguish refractions from the upper/middle crust, marked as the  $P_g$  phase, and refractions from the upper mantle marked as  $P_n$ . Refracted waves from the sedimentary cover ( $P_{\text{sed}}$ ) are observed in the vicinity of shot points in the SE. The first arrivals can usually be correlated up to a distance of 250–300 km. In later arrivals, we observe reflections from the Moho discontinuity ( $PmP$ ) usually as the strongest, reflections from midcrustal discontinuities ( $PiP$ ) and from the top of the lower crust ( $PcP$ ). At large offsets, a reflection from an upper mantle discontinuity ( $P1$ ) can be identified in few shot points. Figures 2a–2c give examples of the whole seismic sections in different parts of the Bohemian Massif, while Figures 3a, 3b, 4a, and 4b show details of the seismic wave field with representative features of the Bohemian Massif, to which we will refer in our following explanation.

### 5.1. $P_g$ Phase

[18] The  $P_g$  phase has an apparent velocity of  $5.8$ – $6.2 \text{ km s}^{-1}$  along the whole profile except at its ends, reflecting the presence of the consolidated Paleozoic basement outcropping at the surface. At the NW end of the profile (0–50 km), lower apparent velocities increasing from  $5.0$  to  $5.9 \text{ km s}^{-1}$  are observed with strong  $P_g$  arrivals (Figure 2a). Similarly, at the SE end (SP 29150, Figure 4b) the first arrivals at offsets smaller than 30 km display an apparent velocity of  $2.5$ – $5.5 \text{ km s}^{-1}$  reflecting several kilometers of sedimentary cover in the Carpathian Foredeep and Neogene basins. Apparent velocities higher than average occur at locations of specific near-surface geological structures, e.g., the apparent velocity of about  $6.1 \text{ km s}^{-1}$  correlates with the mafic Mariánské Lázně Complex at a distance of 115 km along the profile.

[19] For most of the sections from the Bohemian Massif we observe a relatively fast decrease of the  $P_g$  amplitude (e.g., Figure 2c). At offsets of 80–120 km, the  $P_g$  wave becomes either very weak or completely disappears. This phenomenon is visible not only in the trace-normalized sections but also in the true-amplitude sections. Therefore it cannot be explained by the normalization of sections to the maximum trace amplitude, which can make first arrivals hardly visible if they are followed by very strong  $PmP$  reflections. This fact indicates a very small vertical gradient of the  $P$  wave velocity in the upper crust, except in its uppermost (1–2 km thick) part or the existence of a low-velocity zone (LVZ). Another factor contributing to the decaying amplitudes can be relatively high attenuation in the upper crust.

[20] The rate of  $P_g$  amplitude decrease varies. Figure 3a shows an example of a seismic section where the  $P_g$  phase vanishes at about 80 km offset, while for the data from other

locations (Figure 3b), the  $P_g$  phase, though weak, continues at least to 120 km. The first example might be an indication for a LVZ. However, to prove the existence of a low-velocity zone definitely, it should be possible to detect a later phase, corresponding to rays refracted at (or reflected from) the base of the potential LVZ, with an accuracy allowing precise velocity determination. Modeling of such a phase provides a criterion for deciding if a layer with a velocity decrease is really necessary, and for estimating the average velocity in that layer. The later phase visible in Figure 3a is not clear enough to determine its apparent velocity with confidence. Therefore we decided not to introduce a LVZ explicitly and to explain the behavior of the  $P_g$  phase by a very small (close to zero) vertical gradient of the  $V_p$  velocity.

[21] Similar variations of the  $P_g$  amplitudes were observed in other Variscan areas: the Saxothuringian and Moldanubian in Germany [Enderle et al., 1998; DEKORP Research Group, 1988; Zeis et al., 1990], the Massif Central in France [Zeyen et al., 1997], Ireland [Masson et al., 1998] or SW Poland [Grad et al., 2003]. In some cases, they were interpreted as an indication of the existence of a LVZ. Contrasting properties of the  $P_g$  phase (strong amplitudes up to 200 km offset) were observed, e.g., in the crystalline crust of the east European Craton [Środa and Polonaise Profile P3 Working Group, 1999; Czuba et al., 2002; Thybo et al., 2003].

[22] Some sections indicate the continuation of the  $P_g$  phase as secondary arrivals, especially for shots in the middle part of the profile (Figures 2b and 2c). This indicates a low-velocity gradient in the middle crust, which confines refracted arrivals to shallow depth.

### 5.2. Crustal Phases in Later Arrivals and $PmP$ Phase

[23] Besides crustal refracted phases, we also observed reflected waves recorded in later arrivals. Intracrustal reflections ( $PiP$ ) can be observed in several seismic sections, but some of them cannot be traced consistently in more than one section, which makes their interpretation ambiguous. The most widely observed intracrustal reflections occur at offsets of 70–130 km and are thought to originate from a discontinuity at some 15–20 km depth.

[24] In the sections from the NW part of the profile, we observe a clear reflected  $PcP$  phase as the reflection from a deep intracrustal interface, the top of the lower crust (SP 29040, Figures 4a and 2a). This is the strongest reflected phase in these sections, and based on its amplitude and shape it might be interpreted as a reflection from the Moho ( $PmP$ ). Nevertheless, we disallow this interpretation because the arrival time of the observed  $P_n$  wave does not fit the critical point of the discussed phase, as should be the case for refraction and reflection from the same discontinuity. In our data,  $P_n$  phase occurs 1 s later and  $PcP$  phase obscures relatively weak  $PmP$  arriving 0.5–1.0 s later. Also, forward modeling confirmed that hypothesis. Similar observations can be seen in some sections from the GRANU'95 profile [Enderle et al., 1998], which crosses CEL09 at its NW end in the Saxothuringian.

[25] The  $PmP$  phase is the best visible in the central part of the profile roughly corresponding to the Moldanubian unit (SP 29050, 29060 and 29100, Figures 2b and 2c). The critical point, where the  $PmP$  amplitude reaches its maxi-

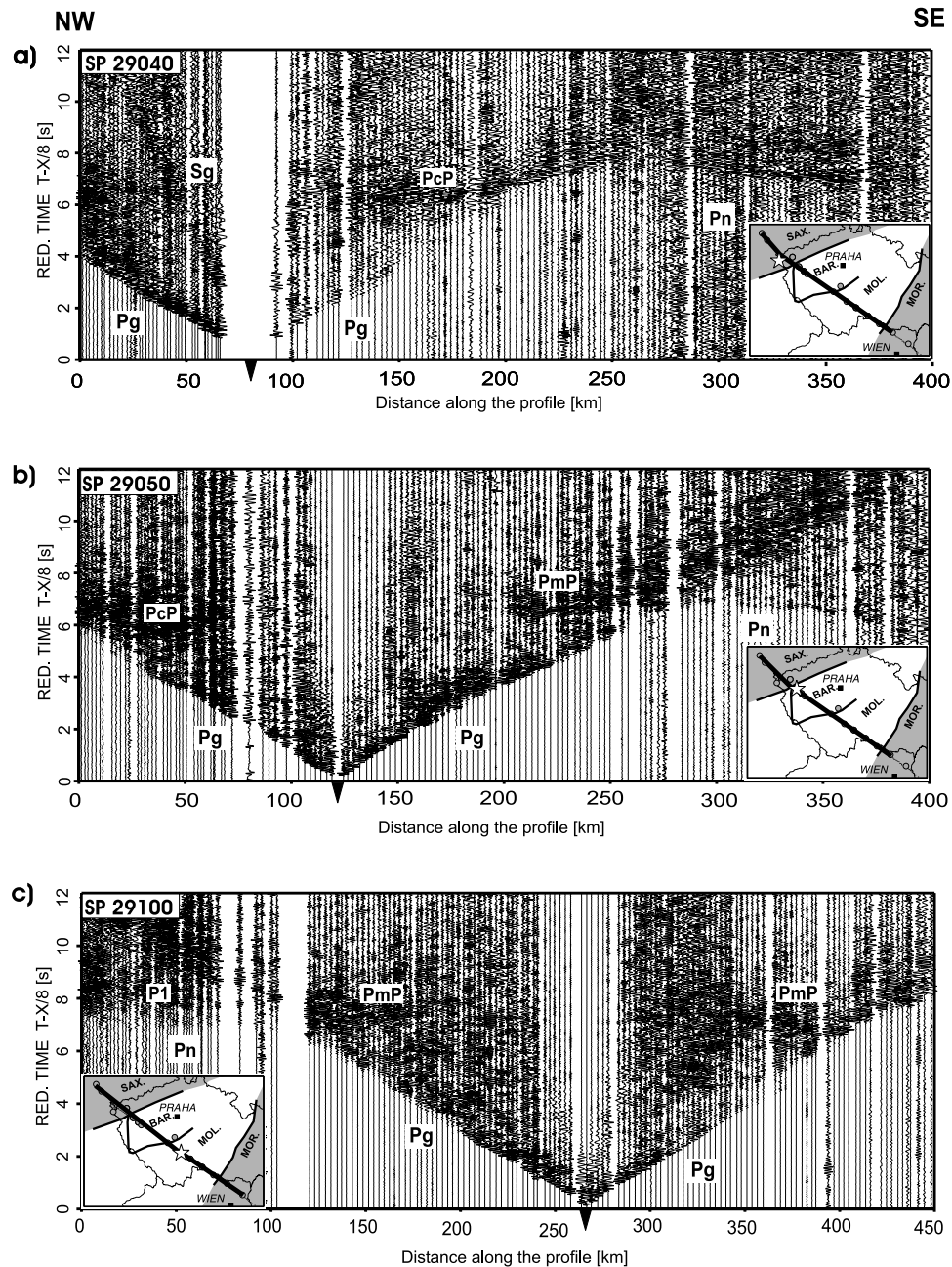


**Figure 2.** Amplitude-normalized vertical component seismic sections for shot points in different parts of the Bohemian Massif plotted with reduction velocity of  $8.0 \text{ km s}^{-1}$ , along with the identifications of the main seismic phases (RED, reduced). *P* waves are *Pg*, refraction within the crust; *Pn*, refraction from the uppermost mantle; *PmP*, reflection from the Moho discontinuity; *PcP*, reflection from the top of the lower crust; and *P1*, mantle reflection. *S* waves are *Sg*, refraction within the crust. Data have been band-pass filtered from 2 to 15 Hz. Locations of major tectonic units and shot points are indicated. (a) SP 29040 (Saxothuringian), strong first *Pg* arrivals in NW, strong *PcP*, weak *PmP* phase in the SE. *Pn* phase is weak but observable. (b) SP 29050 (Moldanubian), no *PmP* observed in the NW, sharp *PmP* and no *PcP* in SE. (c) SP 29100, weak *PmP* phase, scattered reflectivity in the crust, *P1* phase observed.

num, occurs at an offset of about 90–110 km. At larger offsets (up to 250 km), strong overcritical *PmP* arrivals are often observed. In other areas, the *PmP* is weak or not visible (in the NW and SE). This suggests a well-defined Moho discontinuity in the central part of the profile and a transition zone or Moho with relatively low-velocity con-

trast in other parts. In the NW part of the profile (the Saxothuringian), the *PmP* is probably masked by a preceding phase (*PcP*) with much higher amplitude and long coda. The SE end of the profile (beneath the Moravian unit and at the contact of the Bohemian Massif with the Carpathians) exhibits no Moho reflections, no intracrustal reflections (SP

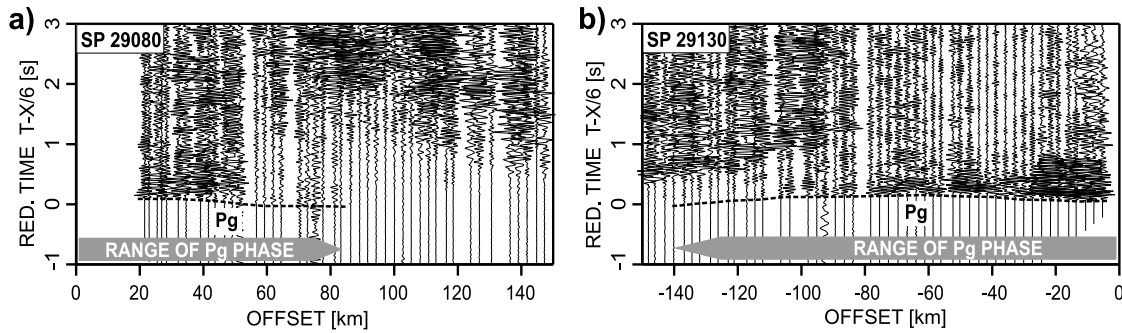


**Figure 3.** Examples of true amplitude vertical component seismic record sections for shot points 29080 and 29130 illustrating differences in the decay rate of the  $P_g$  amplitude. (a) Fast decaying  $P_g$  phase (visible up to 80 km offset). (b) Slowly decaying  $P_g$  wave (observable up to 130 km offset). Reduction velocity is  $6.0 \text{ km s}^{-1}$ , with distance exponent 1.

29150) and strong mantle refraction. This suggests the existence of a zone with gradually increasing velocities, rather than the Moho discontinuity. In this area, the first arrivals display a long coda with high-amplitude oscillations observable within several seconds after the first arrivals. The comparison of the wave field for SP 29150 and SP 29140 (Figure 4b) reveals completely different images: very strong  $P_g$  and  $P_n$  phases for the first section and clear  $P_g$ , very strong  $P_iP$  and weak  $P_n$  for the second section. Taking into account that the distance between the shot points is only 40 km, an abrupt change of the deep crustal structure must occur in this area.

### 5.3. Mantle Phases

[26] The  $P_n$  phase can be identified as first arrivals usually at offsets of 130–230 km, sometimes up to 300 km (Figure 4b) with an apparent velocity of  $8 \text{ km s}^{-1}$  on average. In some sections (e.g., SP 29100, 29110, Figure 2c), a reflected phase following the  $P_n$  phase can be observed at offsets greater than 190 km. We interpreted it as a reflection from a discontinuity in the upper mantle ( $P_1$ ). Though mantle phases are visible only in large distances, the  $P_1$  phase is not observed in all sections with large offsets (e.g., SP 29150, Figure 4b). Thus the corresponding mantle discontinuity seems to be confined to the central part of the Bohemian Massif.

## 6. P Wave Modeling

### 6.1. Seismic Tomography of the First Arrivals

[27] First, we applied the tomographic inversion of Hole [1992] in order to invert the first arrival travel times and determine a smooth 2-D  $P$  wave velocity model. This is a fast tool to assess a preliminary velocity model in the crust. The procedure uses the single backprojection algorithm [Humphreys and Clayton, 1988], based on the linearization of the nonlinear relation between the travel time  $t$  and the slowness  $u = 1/V_p$ . The model is defined on an equidistant rectangular grid; the  $V_p$  velocities are defined at the grid nodes. In the forward step, the travel times are calculated using a finite difference algorithm for solving the eikonal equation [Vidale, 1990], adapted for media with arbitrary velocity variations. The travel time residuals measure the misfit of the model. In the inverse step, the slowness

perturbations are calculated by uniformly distributing the travel time residual along a ray. The perturbations are then summed up for all rays, smoothed and added to the original model. The procedure is repeated iteratively until a model with satisfactory travel time residuals is obtained.

[28] For the inversion, we used 2202 first arrival picks with an uncertainty of  $\sim 50 \text{ ms}$  for most of the  $P_g$  and  $P_n$  phases. The initial 1-D model for the upper crust was calculated by inverting an average travel time curve of  $P_g$  arrivals by the Wiechert-Herglotz formula [Aki and Richards, 1980]; for the lower crust and mantle, a smooth user-defined velocity-depth curve was derived. The 2-D model was calculated for a profile length of 450 km in a uniform grid of  $1 \times 1 \text{ km}$ . The computation was carried out in 6 subsequent steps gradually enlarging the offsets (50, 100, 150, 200, 300, and 400 km) and thus the maximum depth of ray penetration. At each step, several iterations were made with decreasing size of the smoothing area. The smoothing was performed by a moving average filter with cell sizes of  $40 \times 2 \times 10$ ,  $20 \times 2 \times 4$  and  $10 \times 2 \times 2$ . The resolution of the algorithm thus increased gradually and the inversion was stable. The calculation was controlled by the root-mean-square (RMS) travel time residual, which amounted to 80 ms for the final model, exceeding the level of the estimated picking uncertainty by about 50% (Figure 5a).

[29] The residuals, ray coverage, and the resulting tomographic model are presented in Figures 5a–5c. The crust is characterized by an almost uniform velocity distribution throughout most of the Bohemian Massif, except the NW end. The upper crust exhibits a relatively high  $V_p$  gradient in the first 3 km with velocities ranging from  $5.6$  to  $6.0 \text{ km s}^{-1}$  and a very low gradient in the deeper parts with  $V_p$  velocities of  $6.0$ – $6.1 \text{ km s}^{-1}$  down to about 15 km depth. This  $V_p$  distribution corresponds to an almost missing sedimentary cover and outcropping metamorphic and plutonic Paleozoic rocks at the surface. Considerably lower velocities in the upper crust in the range of  $3.0$ – $5.0 \text{ km s}^{-1}$  for depths down to 10 km delimit the beginning of the Carpathian Foredeep in the SE. Because of the high near-surface velocity gradient followed by a low gradient in the upper crust, the turning point of the  $P_g$  rays is at shallow depths (Figure 5b). The rays travel almost horizontally and leave the deeper parts of the crust practically unconstrained.

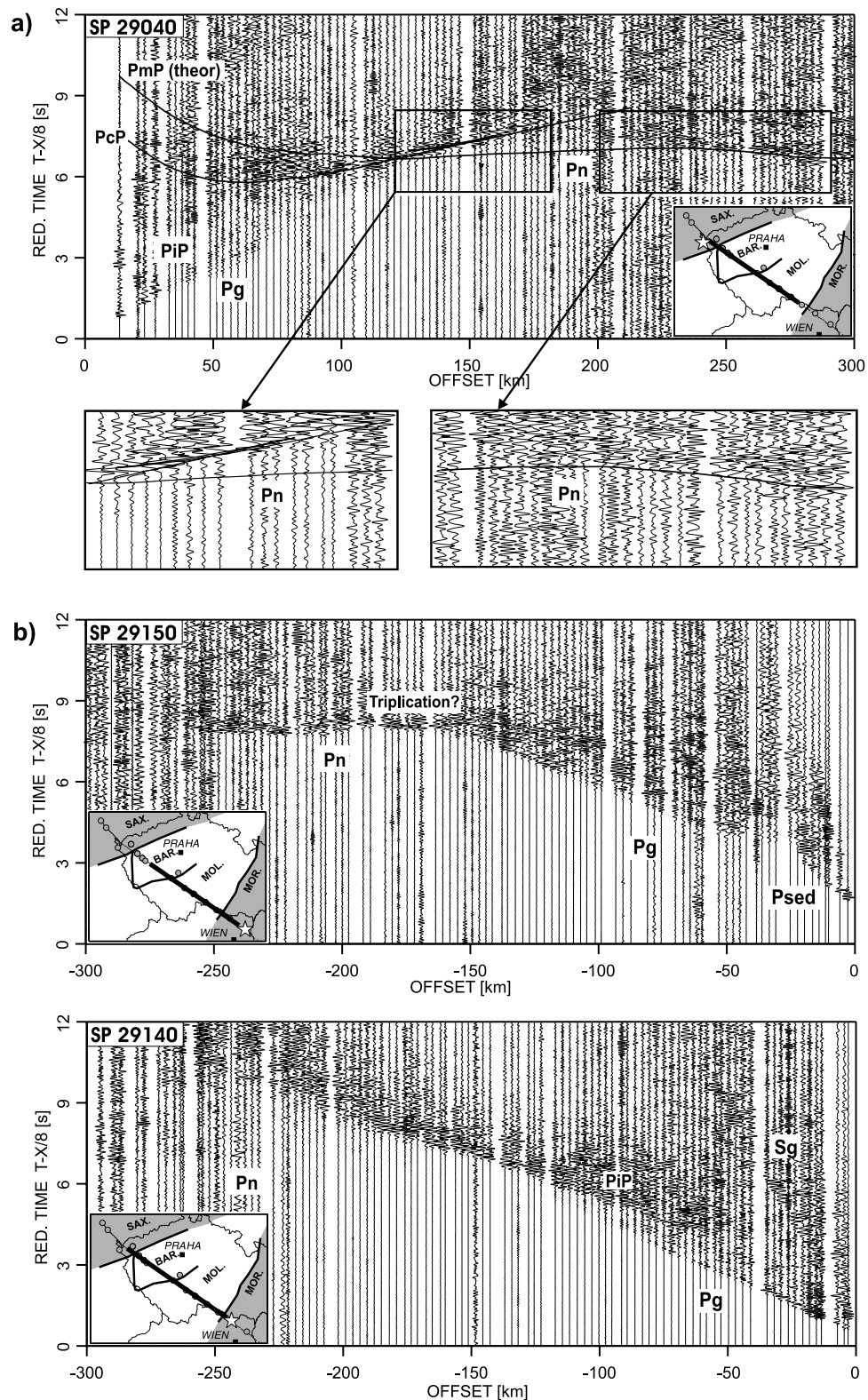


**Figure 4.** Details of amplitude-normalized vertical component seismic sections. (a) SP 29040 in the Saxothuringian, strong  $PcP$  with long coda obscuring the relatively weak  $PmP$  phase. (b) SE end, SP 29150, high-amplitude  $Pn$  phase,  $PmP$  not observed, scattered reflectivity in the crust; SP 29140, no  $PmP$  phase observed, strong  $PiP$ . Description of phases is as in Figure 2, and  $P_{sed}$ , refracted arrivals from the sedimentary cover;  $PiP$ , intracrustal reflection. Reduction velocity is  $8.0 \text{ km s}^{-1}$ .

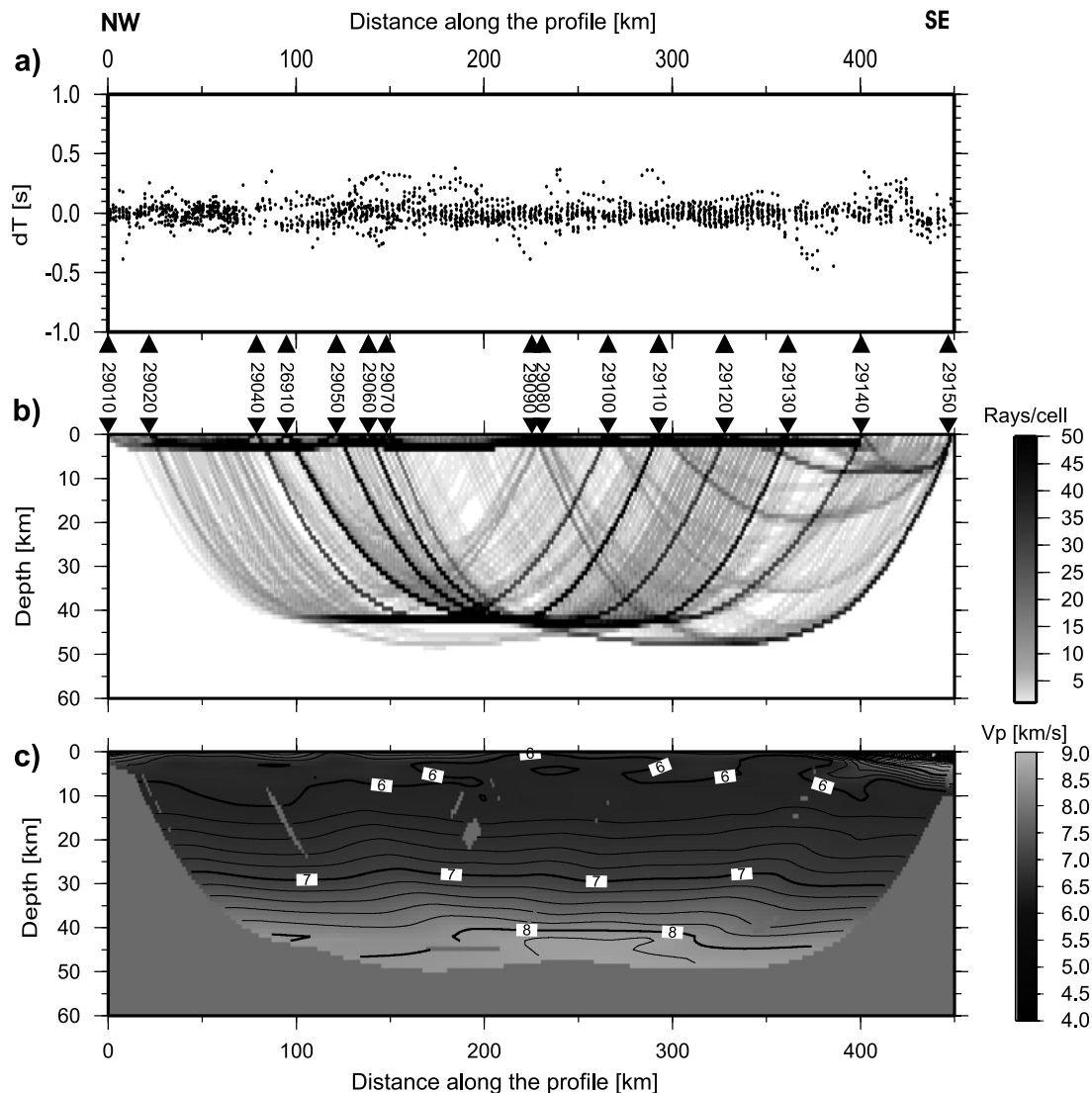


**Figure 5.** Results of 2-D seismic tomography. (a) Misfit between observed and calculated travel times. (b) Ray coverage for the model. (c) Model of  $P$  wave velocity. Triangles indicate shot point positions.

For this reason the middle and lower crust lack any differentiation of velocities in the tomographic model (Figure 5c). Because of the nature of the tomographic algorithm applied, the smoothing performed during the inversion and model parameterization, the velocity discontinuities are smoothed into broad gradient zones and, e.g., the depth of the Moho boundary cannot be reliably estimated.

## 6.2. Trial-and-Error Forward Modeling

[30] The smooth velocity model resulting from the tomographic inversion of the first arrivals (Figure 5) gives only an approximate distribution of velocities in the crust and mantle. On the other hand, modeling of the entire wave field enables a more detailed velocity resolution including velocity contrasts at interfaces and identification of the Moho discontinuity. We thus further refined the 2-D tomographic model by trial-and-error forward modeling using the

SEIS83 program package [Červený and Pšenčík, 1984]. In this modeling approach, to obtain the  $P$  wave velocity distribution, we used not only the first arrivals but also further phases (reflected waves and available refractions in later arrivals). The modeling also involved the calculation of synthetic sections and qualitative comparison of amplitudes of synthetic and observed seismograms. Since the amplitudes of seismic waves are very sensitive to velocity gradients and velocity contrasts at discontinuities, synthetic seismograms of both reflected and refracted seismic waves were useful tools in obtaining additional constraints on the velocity distribution.

[31] The SEIS83 algorithm calculated ray paths, travel times and synthetic seismograms in the high-frequency approximation. The model consisted of layers separated by velocity discontinuities. In each layer, the  $P$  wave velocity was specified in an irregular rectangular grid and interpolated by bicubic splines. The solution was

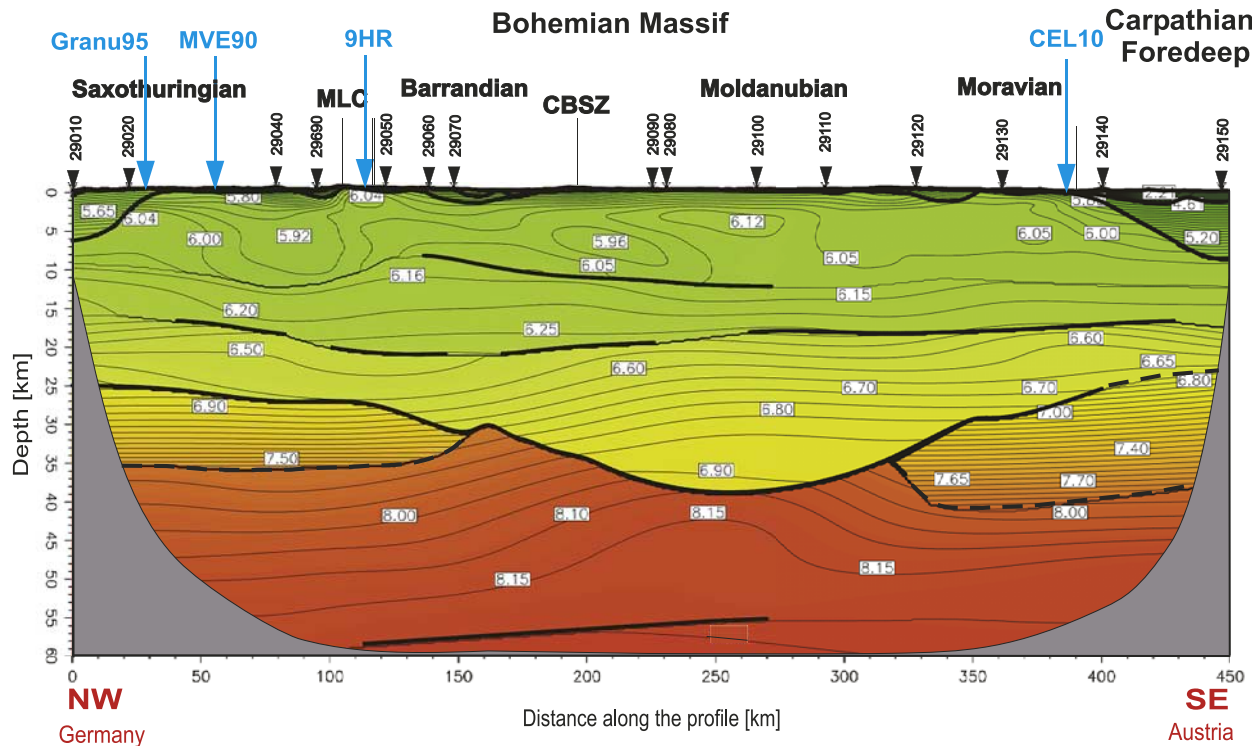


**Figure 6.** The 2-D model of the  $P$  wave velocity along the CEL09 profile developed by forward ray-tracing modeling (with SEIS83). The gray covers the unconstrained parts of the model. Bold lines mark boundaries constrained by reflections and well-constrained interfaces in the uppermost crust; dashed bold lines mark layer boundaries where no reflections were observed. Thin lines represent velocity isolines spaced at intervals of  $0.05 \text{ km s}^{-1}$ . Triangles show projections of the shot points. Arrows show the locations of other refraction and reflection profiles. MLC, Mariánské Lázně Complex; CBSZ, Central Bohemian Shear Zone. Vertical exaggeration is 1:3.

sought iteratively: the travel times of the refracted and reflected waves were calculated for the current  $V_p$  model and compared with the observed travel times. Then the  $V_p$  model was changed in order to minimize the misfit.

[32] The final 2-D model of the  $P$  wave velocity distribution is presented in Figure 6. In accordance with the tomography model, the upper crust of the Bohemian Massif displays a relatively high  $V_p$  gradient in a near-surface 2–3 km thick zone with velocities of 5.8–6.0  $\text{km s}^{-1}$ , except at its NW end. The first, high-gradient layer with velocities of 5.8–6.0  $\text{km s}^{-1}$  is the most pronounced in the Barrandian and Saxothuringian, while the Moldanubian and Moravian units show an almost constant near-surface velocity of 6.0  $\text{km s}^{-1}$ . Lower  $V_p$  velocities, characteristic for sedimentary rocks with velocities ranging from 5.0 to 6.0  $\text{km s}^{-1}$  to  $\sim 6$  km depth, occur in the NW. Mafic Mariánské Lázně Complex exhibits near-surface velocity of  $V_p$  6.05  $\text{km s}^{-1}$  at a distance of 115 km along the profile. The SE part of the profile from 400 km onward reflects a sedimentary cover of the Carpathian Foredeep at the eastern edge of the Bohemian Massif with velocities in the range of 2.5–5.5  $\text{km s}^{-1}$  to a depth of about 10 km.

[33] Deeper parts of the upper crust, not resolved properly by the tomography, exhibit a very low vertical gradient with the  $V_p$  velocity of 6.0–6.1  $\text{km s}^{-1}$  down to about a depth of 13 km. This low gradient is evidenced

by the fast decrease of  $Pg$  wave amplitude for most of the shot points. The alternative solution may involve introduction of a low-velocity layer in the upper crust, however, in our opinion the data did not allow the evaluation of the amount of velocity decrease, and therefore we decided not to propose it. In the middle crust, we identified two reflectors with a velocity contrast of 0.15–0.3  $\text{km s}^{-1}$  in the depth ranges of 8–13 km and 17–20 km ( $PiP$  phases). The upper one is limited to the central part of the Bohemian Massif, to distances among 150–270 km along the profile, slightly dipping to the SE. The lower one is detectable with gaps almost throughout the whole massif.

[34] The most distinct lateral differences in  $V_p$  velocities in the Bohemian Massif can be distinguished in the lower crust. According to its properties and the character of the crust-mantle transition zone, the investigated area can be divided into three areas: (1) the central part of the Bohemian Massif, which correlates with the extent of the Moldanubian, (2) the NW part in the Saxothuringian, and (3) the SE part beneath the Moravian.

[35] In the Moldanubian, the  $PmP$  phase is the most pronounced in terms of high amplitude and short pulse length, and Moho is interpreted as a first-order discontinuity (from 6.9 to 8.1  $\text{km s}^{-1}$ , see Figure 7a). The maximum Moho depth is 39 km. The  $V_p$  velocity in the middle and lower crust increases gradually from 6.5  $\text{km s}^{-1}$  at 19 km

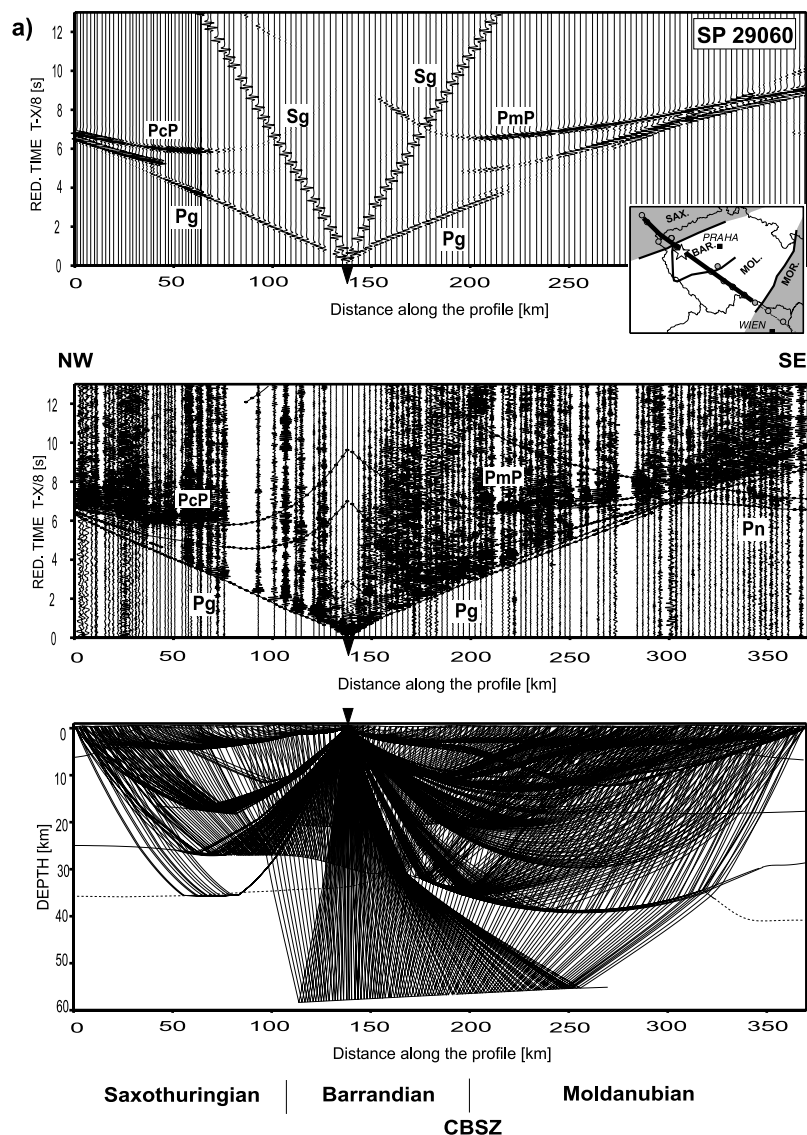


**Figure 7.** Examples illustrating forward modeling for selected shot points. (bottom) Model and ray paths, (middle) seismic record sections with superimposed calculated travel time curves (solid lines) for final model, and (top) synthetic seismic sections. (a) SP 29060, documentation of the Moho discontinuity in the Moldanubian, (b) SP 29150 documentation of gradient zone in the SE, and (c) SP 29110 and 29100, documentation of the mantle reflector. Reduction velocity is  $8 \text{ km s}^{-1}$ .

depth to  $6.9 \text{ km s}^{-1}$  above Moho, without any pronounced discontinuities in this depth range. The upper mantle velocities of  $8.0\text{--}8.15 \text{ km s}^{-1}$  are higher than in the neighboring units.

[36] In the Saxothuringian and partly beneath the Barrandian in the NW to a distance of 150 km along the profile, a lower crustal layer with a velocity gradient from  $6.9$  to  $7.5 \text{ km s}^{-1}$  can be inferred above the Moho. The character of the reflection from the top of the lower crust (*PcP* phase) with the long and irregular coda indicates that the layer is highly reflective, probably due to the presence of thin layers of material with contrasting seismic velocities. The properties of this layer were investigated in detail by synthetic seismogram modeling using the reflectivity method and will be discussed later. The top of this layer is located at a depth of  $25\text{--}27 \text{ km}$

and is explained by the interface with a velocity contrast of  $0.3 \text{ km s}^{-1}$ . The bottom is interpreted to have a smaller velocity contrast at the Moho in order to obtain low amplitudes of the *PmP* phase as compared to the *PcP*, as observed in the data (Figures 2a and 4a). Since no refracted phase from this layer is observed and the *PmP* phase is poorly visible, the velocities in the lower crust are not well constrained and they are inferred only by modeling of the amplitude relation of the *PcP* to Moho reflections.

[37] The Moravian unit exhibits no distinct intracrustal reflectors except for the discontinuity at a depth of  $18 \text{ km}$ , which is the most pronounced at a distance of about  $350 \text{ km}$  along the profile and which produces a very strong reflection for SP 29140. The Moho reflection, however, is not visible (Figure 4b). The section in the very SE (SP 29150)

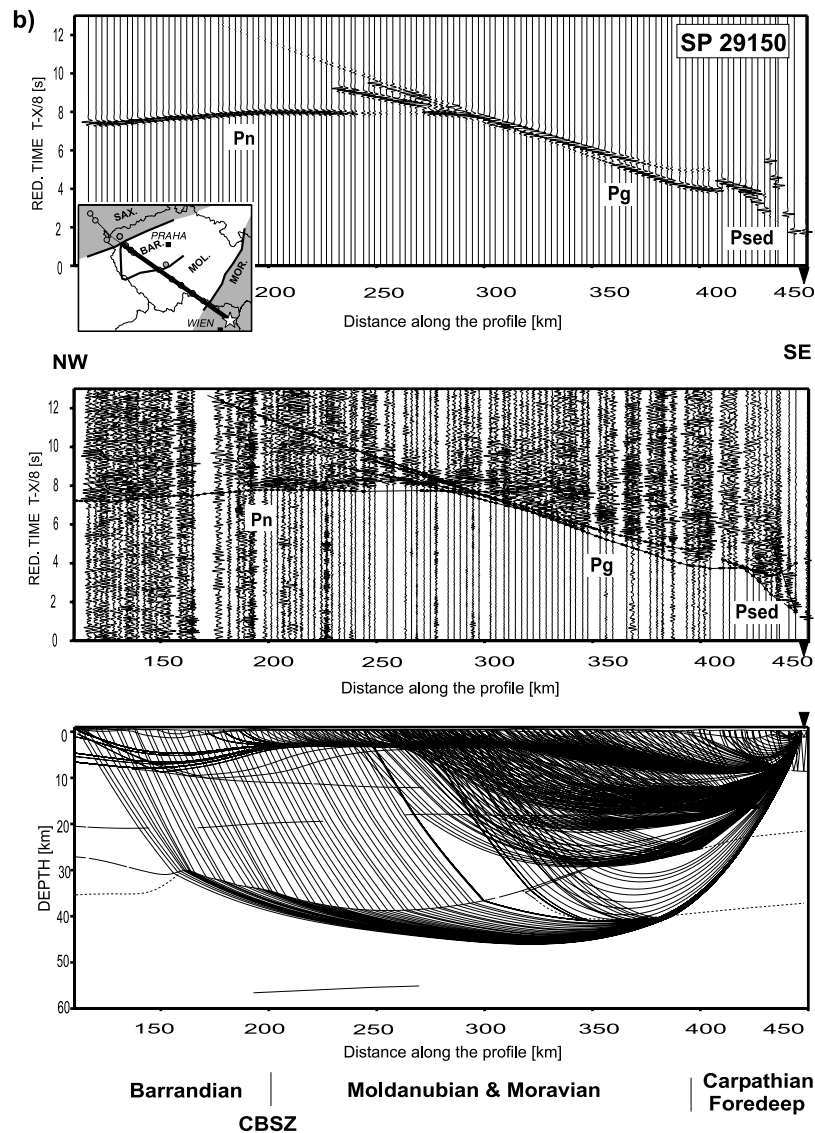


Figure 7. (continued)

exhibits quite unusual character: only the first arrivals can be clearly identified as a strong  $Pg$  turning into a very strong  $Pn$  phase. Apart from this, we identified a weak phase with a high apparent velocity in a short offset interval (140–180 km), immediately after the bending point of the first arrivals (place where  $Pg$  phase turns into  $Pn$  phase), forming a triplication. Travel time curves have this shape in media without velocity discontinuities but with a vertical gradient increase at some depth. Therefore, on the basis of the results of 1- and 2-D modeling of travel times and amplitudes, we suggest that the lower crust and crust-mantle transition in this area is a 17 km thick gradient zone at depths of 23–40 km with  $V_p$  velocities ranging from 6.8 to 7.8 km s<sup>-1</sup> (Figure 7b). The top and bottom of this zone are interpreted with no distinct velocity discontinuities, especially in the very SE part. Therefore in this part of the model there is no Moho discontinuity but a thick crust-mantle transition zone. The uppermost mantle displays a velocity of 7.9 km s<sup>-1</sup>.

[38] Mantle velocities in the Bohemian Massif range from 7.85–8.15 km s<sup>-1</sup>, with the highest and well-constrained values in the central part in the Moldanubian. Upper mantle velocities of about 7.9 km s<sup>-1</sup> in the NW and 8.0 km s<sup>-1</sup> in the SE were derived with higher uncertainty. A local mantle reflector (at a distance of 115–265 km), slightly dipping to the NW, is visible at a depth of 55–58 km (Figure 7c). Velocities beneath this reflector are not constrained, as no arrivals are observed from below it.

### 6.3. Analysis of Resolution and Uncertainties

[39] Uncertainties for any 2-D seismic velocity model are due to a combination of several factors. Some amount of subjectivity cannot be avoided but the model accounts for the major features observed in the seismic data. Errors and uncertainties originate in travel time picking errors, misinterpretation of seismic phases and inaccuracy of modeling (misfit between data and modeled travel times), amount of data, geometry of the experiment and simplification of the

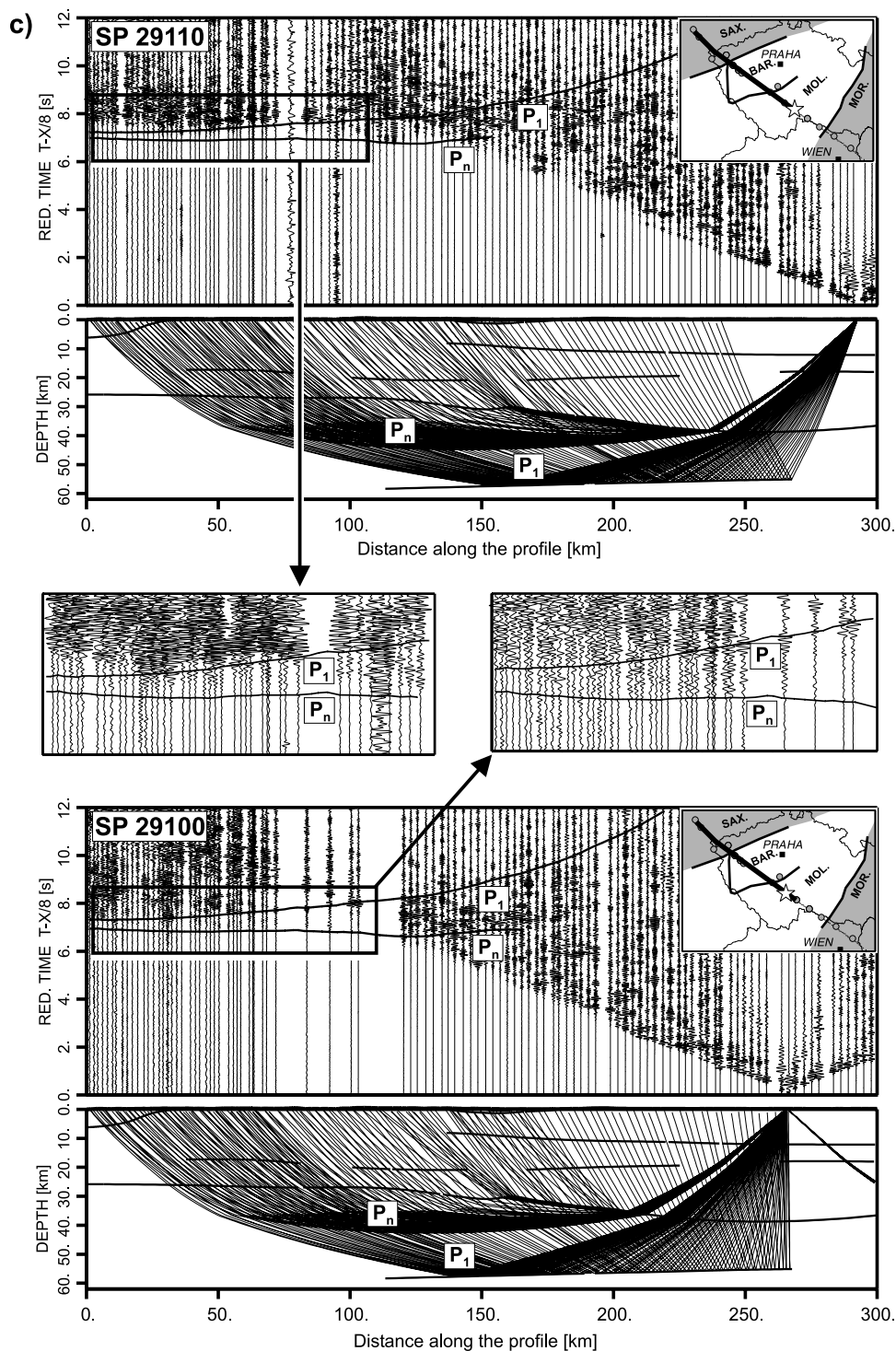
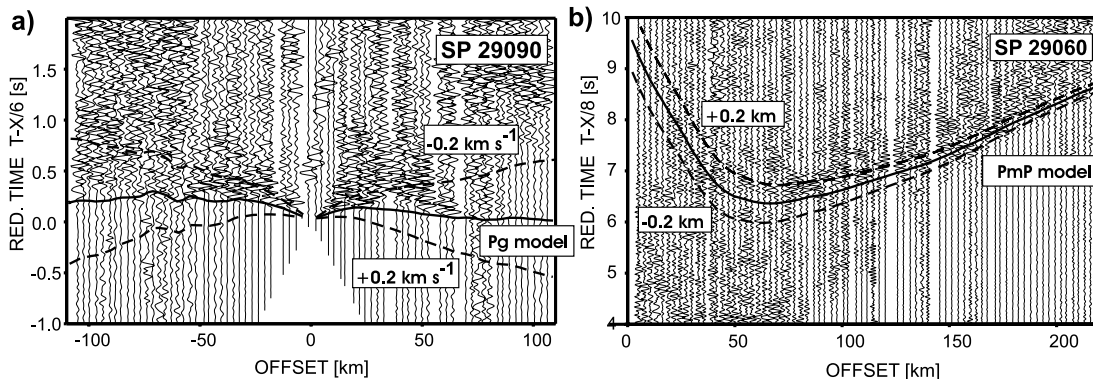


Figure 7. (continued)

model where 3-D effects or anisotropy are not considered. Also, the limitations of the ray theory must be kept in mind. Since the errors introduced by the interpreter during correlation and interpretation of seismic phases are subjective and impossible to quantify, it is not possible to perform a systematic error analysis.

[40] Figure 8a shows an approximate estimation of the differences in the calculated travel times of  $P_g$  waves.

The response of the presented model (Figure 6) and the response for the model with the  $P_g$  velocity perturbations of  $\pm 0.2 \text{ km s}^{-1}$  (about 3%) are depicted. Figure 8b shows an approximate estimation of the differences in the calculated travel times of  $P_mP$  waves. It is clear that the uncertainties of the apparent velocity determination based on the first arrivals are much less than  $\pm 0.2 \text{ km s}^{-1}$ , and similarly, this suggests that the uncertainties in the



**Figure 8.** Estimation of model uncertainties. (a) Seismic section for shot point SP 29090 with calculated travel times for the *Pg* phase with velocity model shown in Figure 6 (solid line) and differences in travel times for the model with the upper crustal velocity different by  $\pm 0.2 \text{ km s}^{-1}$  (dashed lines). Reduction velocity is  $6.0 \text{ km s}^{-1}$ . (b) Seismic section for shot point SP 29060 with calculated travel times for the *PmP* phase with the velocity model shown in Figure 6 (solid line) and differences in travel times for the model with the location of Moho different by  $\pm 2 \text{ km}$  (dashed lines). Reduction velocity is  $8.0 \text{ km s}^{-1}$ .

depth of Moho (and intracrustal reflectors) are less than  $\pm 2 \text{ km}$ .

### 7. Analysis of S Waves

[41] Some of the recorded seismic data show an *S* wave signal for refracted crustal phases (*Sg*) and reflected phases from Moho (*SmS*). Seismic sections show recordings with

clear arrivals of *Sg* phase with an apparent velocity of  $3.5 \text{ km s}^{-1}$  and *SmS* waves up to an epicentral distance of 230–350 km. Neither intracrustal and mantle reflections nor Moho refraction, could be reliably identified (Figure 9). Altogether, refracted and reflected *S* wave arrivals have been correlated in 15 seismic sections. The recordings of the vertical component were used for *S* waves interpretation, as the horizontal component was recorded by a small number

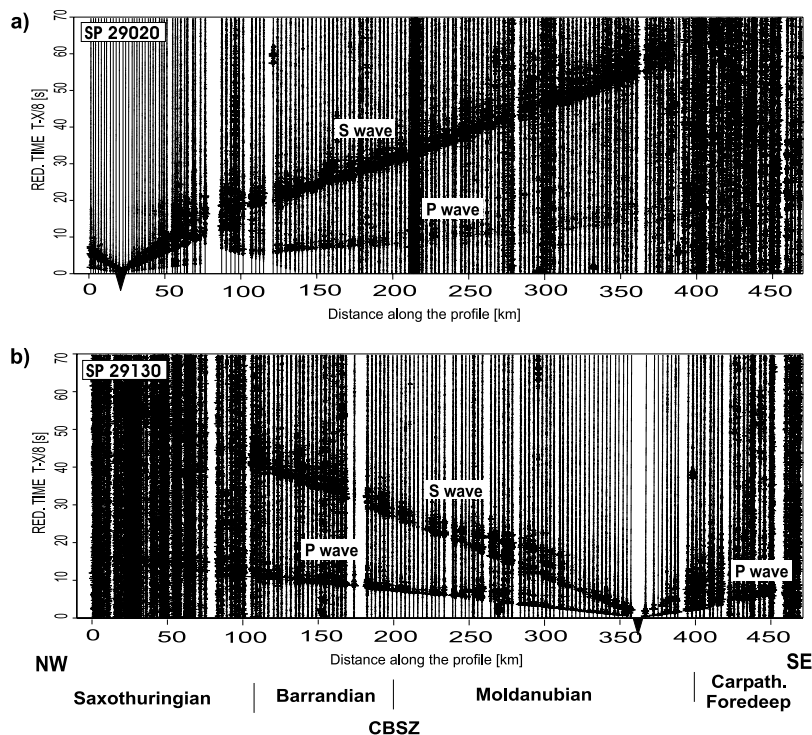


**Figure 9.** Examples of amplitude-normalized vertical component seismic sections for (a) SP 29020 and (b) SP 29130, along with the identifications of the main seismic phases of *P* and *S* waves. Reduction velocity is  $8.0 \text{ km s}^{-1}$ . A 2–10 Hz band-pass filter was applied.

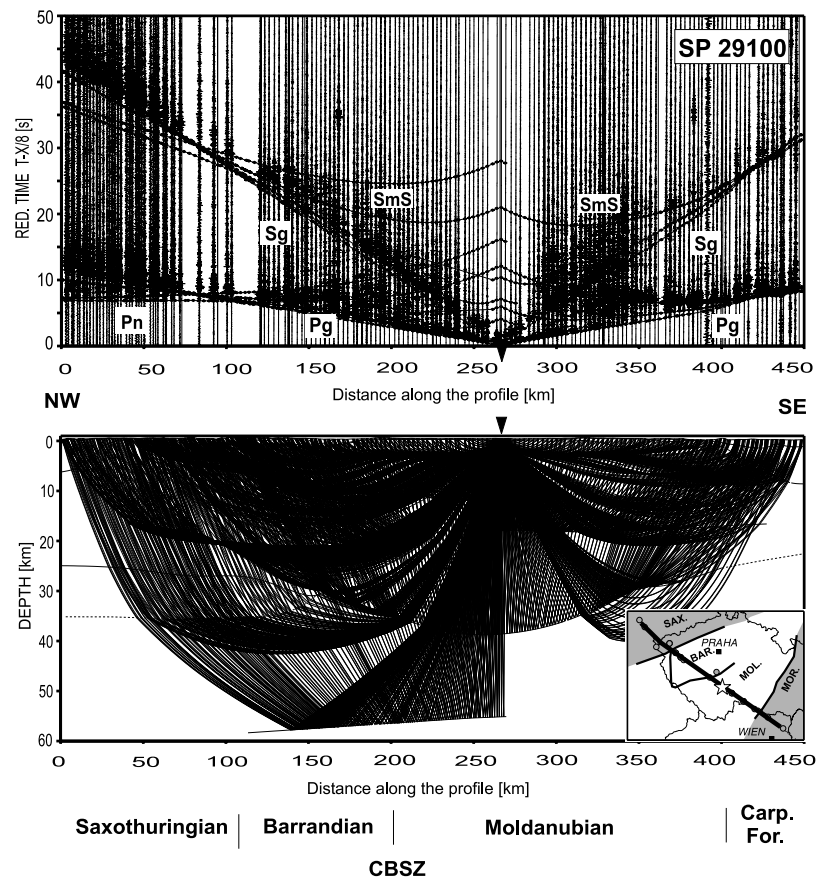


**Figure 10.** Example of  $P$  and  $S$  wave forward modeling for shot point SP 29100. (top) Model and ray paths; (bottom) seismic record sections with superimposed calculated travel time curves (solid line) for the final model.  $V_p/V_s$  ratio is 1.73. Seismic data section is shown with the same parameters and phase description as in Figure 2. Reduction velocity is  $8 \text{ km s}^{-1}$ .

of stations. Nevertheless, the vertical component shows as clear shear wave arrivals as the horizontal components, which is often the case with crustal refraction data [see, e.g., Thybo *et al.*, 2003]. In the middle part of the Bohemian Massif, the observed first  $S$  wave arrivals ( $S_g$ ) at larger offsets (80–150 km) are weak compared to  $S$  wave reflected arrivals, which is similar to the effect of the  $P_g$  phase in that area. Similar to the  $P$  wave, it again indicates a small velocity gradient in the upper crustal parts. In the NW, we can observe  $ScS$  phase (reflection from the top of the lower crust) with a long coda, indicating that the lower crust is reflective for  $S$  waves too.

[42] The best branches of correlated  $S$  wave travel times were used for forward modeling to provide another constraint in discriminating different tectonic areas. The  $S$  wave velocity model in the first approximation was adopted from the  $P$  wave model and converted into the  $V_s$  velocity model using the standard ratio of  $V_p/V_s = 1.73$  [e.g., Christensen, 1996]. Lack of reflected crustal arrivals, as well as refractions from the upper mantle, together with the limited number of good quality travel time picks obtained did not allow detailed  $S$  wave modeling, and thus the obtained accuracy did not enable fine variations of the  $V_p/V_s$  ratio to be determined throughout the model. Forward modeling of the  $S$  wave travel times for available refracted ( $S_g$ ) and reflected ( $SmS$ ) phases for the given model did not indicate

that  $V_p/V_s$  differs substantially from 1.73 along the profile (Figure 10). The only exception can be found for the upper crust at the distance of 150–230 km along the profile, where slightly higher values of the  $V_p/V_s$  ratio (1.76) can be observed. Such lower  $S$  velocity values may suggest slightly higher density of cracks or fluid-filled fractures in that area roughly spreading along the Central Bohemian Shear Zone (at the distance of 200 km along the profile).

## 8. Modeling of Lower Crustal and Moho Characteristics by the Reflectivity Method

[43] During forward modeling we observed differences in the amplitudes and coda length of some reflected phases that were not possible to analyze by the ray-tracing modeling. Therefore we used the reflectivity method by Fuchs and Müller [1971] to simulate the variability of the character of the lower crust and Moho reflections assuming a 1-D seismic velocity-depth structure. On the basis of the result of 2-D forward modeling we took representative 1-D functions from three different areas and tested them for the existence of features such as laminated layers with alternating high and low velocities or high gradient zones. For three representative seismic sections (SP 29040, 29050, and 29150), we calculated synthetic seismograms and compared the seismic data with these synthetic seismograms (see Figure 11).

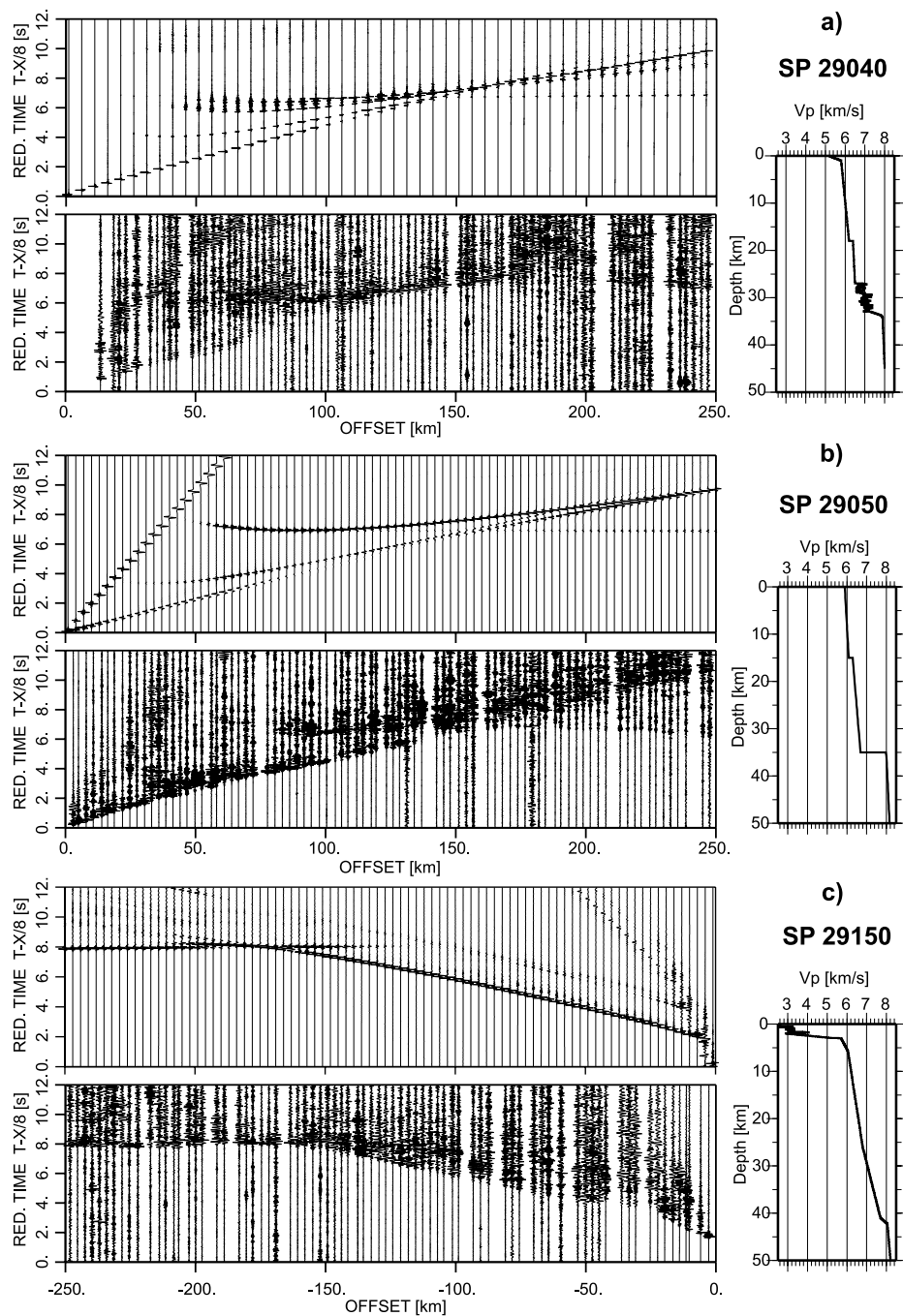


**Figure 11.** Modeling of the lower crustal and Moho characteristics using the reflectivity method. (top) Synthetic reflectivity seismograms and (bottom) seismic data; (right) 1-D velocity model. Seismograms and seismic data sections are shown with the same scaling parameters as in Figure 2. (a) SP 29040, Saxothuringian area (NW). Strong reflections form the top of the lower crust ( $PcP$ ) and from the laminated lower crust, with the coda obscuring the  $PmP$  phase, weak  $Pn$ . (b) SP 29050, Moldanubian area. No  $PcP$  phase, sharp Moho reflection ( $PmP$ ), no evidence of the laminated lower crust. Interpreted as strong Moho discontinuity with the velocity contrast. (c) SP 29150, SE edge of the Bohemian Massif. Very strong and ringing first arrivals ( $Pg$  and  $Pn$ ). Interpreted as a thick gradient zone.

[44] Section 29040 (Figure 11a), recorded in the area of the Saxothuringian (NW), displays a high-amplitude reflection from the top of the lower crust, with a long coda suggesting strong reflectivity of the lower crustal layer. The coda obscures a relatively weak *PmP* phase. The *Pn* phase is weak, but observable. The proposed 1-D model explains it by the existence of the lower crustal layer with a background  $V_p$  velocity of 6.9–7.3 km s<sup>-1</sup>, consisting of layers of randomly alternating high and low velocities with a standard deviation of 4% and correlation length of 300 m. Moho is interpreted as a 1 km thick gradient zone at a depth of 33 km with velocities increasing gradually from 7.3 to 7.9 km s<sup>-1</sup>, which produces a refracted phase weak enough to fit the data.

[45] The section from SP 29050 (Figure 11b), located in the Moldanubian area, shows relatively sharp onsets of the *PmP* phase and a clear *Pn* phase. The high-velocity reflective lower crust is absent in the model and Moho is suggested to be a discontinuity with a velocity contrast from 6.8 to 8.1 km s<sup>-1</sup>.

[46] The section from SP 29150 (Figure 11c), recorded at the SE edge of the Bohemian Massif, differs from all other data along the profile, and bears some resemblance to few sections from the CEL10 profile of the CELEBRATION 2000 experiment (under interpretation). Strong first arrivals, including the *Pn* phase, were observed up to the offsets of 300 km, but the *PmP* phase is not visible. Also no clear intracrustal reflections are visible. Thus the lower crust is interpreted as a thick layer with a high gradient of  $V_p$  velocities from the lower crust to the uppermost mantle. Such a gradient zone may represent a broad transition zone between the crust and mantle. The overall ringing character of the data and long coda (high amplitude oscillations observable within a few seconds after the first arrivals) may be explained by a high reflectivity caused by small-scale velocity fluctuations in the thick sedimentary sequences beneath the shot point. The long coda can also be explained as due to the overall increased reflectivity of the Moravian basement.

## 9. Gravity Modeling

[47] After interpretation of seismic velocities, we used gravity modeling to test the seismic model and to obtain additional geophysical constraints on the crustal structure and composition. In the first approximation we converted the *P* wave velocity model (Figure 6) into density blocks using a velocity-density relation of *Thybo and Schönharting* [1991] and created an initial density model. Using the 2-D modeling software GRAVMOD developed by *Zelt* [1994], we compared the gravity effect of this initial density model with Bouguer anomalies along the profile. We then modified the densities in model blocks where needed by trial-and-error in order to obtain a better fit to experimental gravity data.

[48] Figure 12a shows Bouguer anomalies together with the gravity response of the initial density model and resulting final model. The analysis of the gravity response for the initial model (Figure 12b) indicates that the seismic model agrees with Bouguer anomalies in terms of the large-scale and deeper structure because the calculated gravity effect resembles a long-wavelength, smoothed version of the

experimental gravity values. The most prominent discrepancy (about 50 mGal) occurs in the distance range of 60–120 km along the profile, where the negative anomaly reaches –60 mGal. This minimum coincides with the location of the granitoid Karlovy Vary Pluton, mostly located slightly to the NE of the CEL09 profile. Therefore the discrepancy for the initial model is probably due to the larger density difference between the Karlovy Vary granites and surrounding rocks than estimated from seismic velocities. Another contributing factor might be a 3-D influence of the density anomalies, not taken into account by the 2-D velocity modeling. However, the aim was to test 2-D velocity results, therefore we confined the gravity modeling to two dimensions.

[49] The final density model (Figure 12c) explains discrepancies in the short-wavelength anomalies, which results in a better fit of the corresponding gravity curve. The modifications were mostly confined to the upper crust, with the biggest changes in the Karlovy Vary area. There, the difference between the granitoids and neighboring metamorphic rocks is more pronounced in density (about 0.1 g cm<sup>-3</sup>) than in seismic velocities, consistently with the results of *DEKORP Research Group* [1994]. Other, smaller corrections (positive and negative) were made in most parts of the upper crust, explaining the anomalies caused by numerous granitoid plutons, as well as mafic rocks, occurring along the profile or in its close vicinity and producing a gravity effect not accounted for by velocity modeling.

## 10. Interpretation and Discussion of the Results

[50] The CELEBRATION 2000 profile CEL09 was designed to cross the key tectonic units of the Bohemian Massif. Figure 13 summarizes the main interpreted features of the crust and uppermost mantle together with the 1-D velocity characteristics for different parts of the Bohemian Massif and suggests possible tectonic interpretation of velocity and gravity models that we discuss in detail in this section. In general, the average overall compressional velocity of the crust in the Bohemian Massif is about 6.3 km s<sup>-1</sup> and is slightly lower than the crustal average of 6.45 km s<sup>-1</sup> presented by *Christensen and Mooney* [1995] for the continental crust. Even then, it is still higher than the average of 6.0–6.2 km s<sup>-1</sup> observed in the Moldanubian and Saxothuringian in SW Germany [*Giese*, 1976].

### 10.1. Upper Crust

[51] The upper crust shows relatively small lateral variations of  $V_p$  (except for younger formations at both ends of the profile); nevertheless, the large-scale velocity anomalies may be correlated with the composition of the individual tectonic units. We believe that in this case even relatively small velocity differences may be meaningful because the uppermost part of the model is best resolved due to the maximum ray density in this depth range.

[52] In the uppermost crust, the Barrandian and Saxothuringian show a high-gradient layer with velocities of 5.8–5.9 km s<sup>-1</sup> down to a depth of 3 km, which may be connected with volcano-sedimentary and sedimentary Lower Paleozoic rocks. The metamorphic rocks and Variscan granitoid intrusions in the Moldanubian are characterized by a similar velocity increase of 5.9–6.0 km s<sup>-1</sup> down

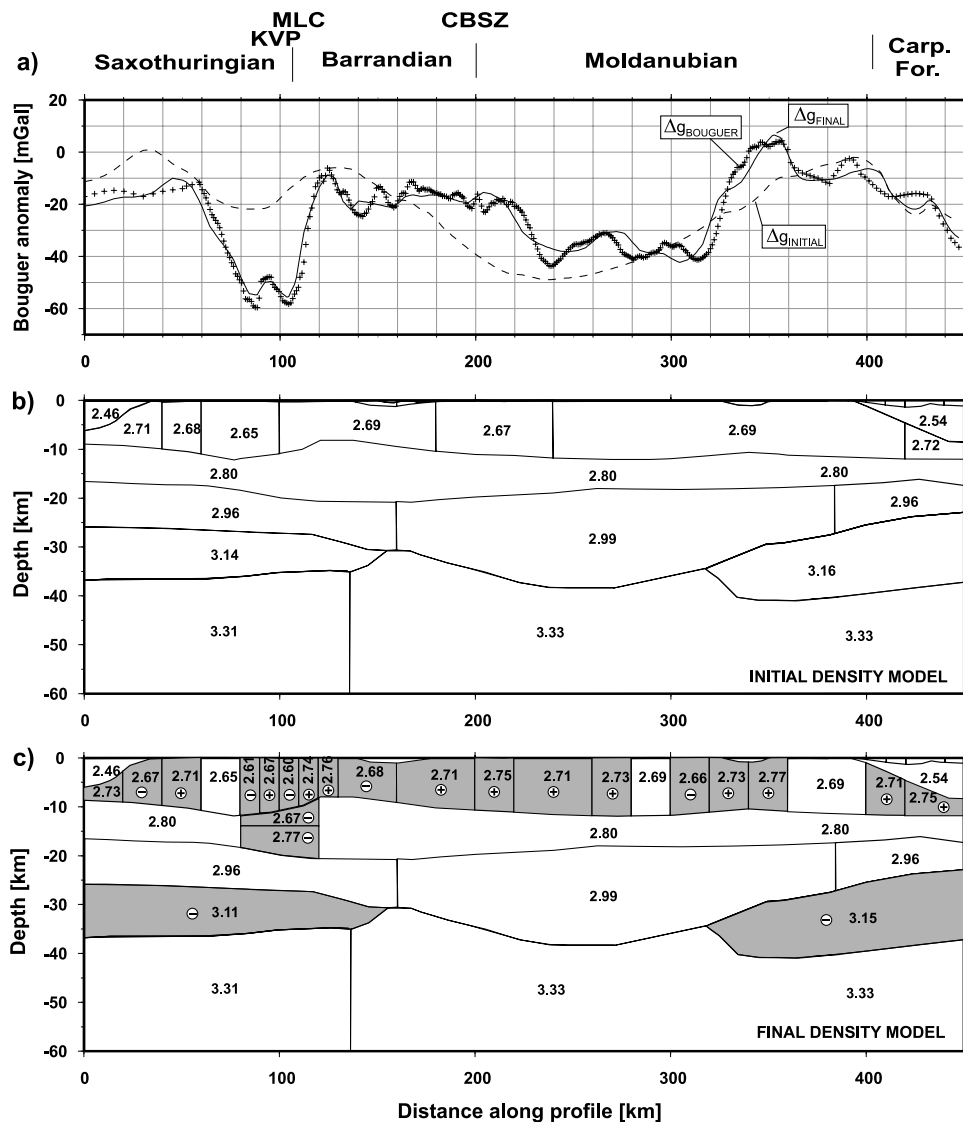


**Figure 12.** Gravity modeling. (a) Bouguer anomaly (crosses), calculated gravity effect from initial density model (dashed line) and from final density model (solid line). (b) Initial gravity model converted from seismic velocity model in Figure 6. (c) Final gravity model. Blocks with densities different from initial model are marked in gray. Signs in circles represent positive or negative density modifications. Numbers in blocks indicate densities in  $\text{g cm}^{-3}$ . Geological abbreviations are MLC, Mariánské Lázně Complex; KVP, Karlovy Vary Pluton; CBSZ, Central Bohemian Shear Zone.

to a depth of 2 km due to the closing of microcracks under increasing pressure [Pros *et al.*, 1998]. In deeper parts of the upper crust down to about 13 km, the vertical velocity gradient is very small (velocity increase of  $0.05\text{--}0.1 \text{ km s}^{-1}$  over an interval of 10 km), as indicated by a fast decay of the  $P_g$  wave amplitude. In terms of horizontal variability, a slightly smaller  $V_p$  velocity ( $5.9\text{--}6.0 \text{ km s}^{-1}$ ) characterizes the Saxothuringian Paleozoic sediments, and possibly also the granitoids of the Karlovy Vary intrusion at a distance of around 90 km along the profile. The latter, even if not as pronounced in terms of velocities, produces a significant (about  $0.1 \text{ g cm}^{-3}$ ) density contrast with respect to neighboring areas. Similar  $V_p$  velocities characterize the upper crust of the Barrandian unit. Slightly higher velocities occur in the Moldanubian, especially in its central part (up to  $6.1 \text{ km s}^{-1}$ ), abundant in high-grade gneisses and

migmatites of the crystalline basement. Lower velocities ( $5.95 \text{ km s}^{-1}$ ) at a distance of 200–230 km along the profile and depth of 10 km may be connected with the intrusion of the granitoid Central Bohemian Pluton.

[53] Local near-surface velocities of  $6.05 \text{ km s}^{-1}$  and densities with a density contrast of  $0.1 \text{ g cm}^{-3}$  observed in the area of the amphibolite Mariánské Lázně Complex at the boundary between the Saxothuringian and Barrandian are smaller than those expected for a body of mafic composition. Possible reason is that the profile crosses only a thin portion of the complex at its NE end, and thus it has only a moderate influence on the apparent velocities of the refracted arrivals.

[54] More pronounced  $V_p$  variations in the upper crust were observed in the NW part of the Saxothuringian. They show velocities of  $5.0 \text{ km s}^{-1}$  at the surface increasing

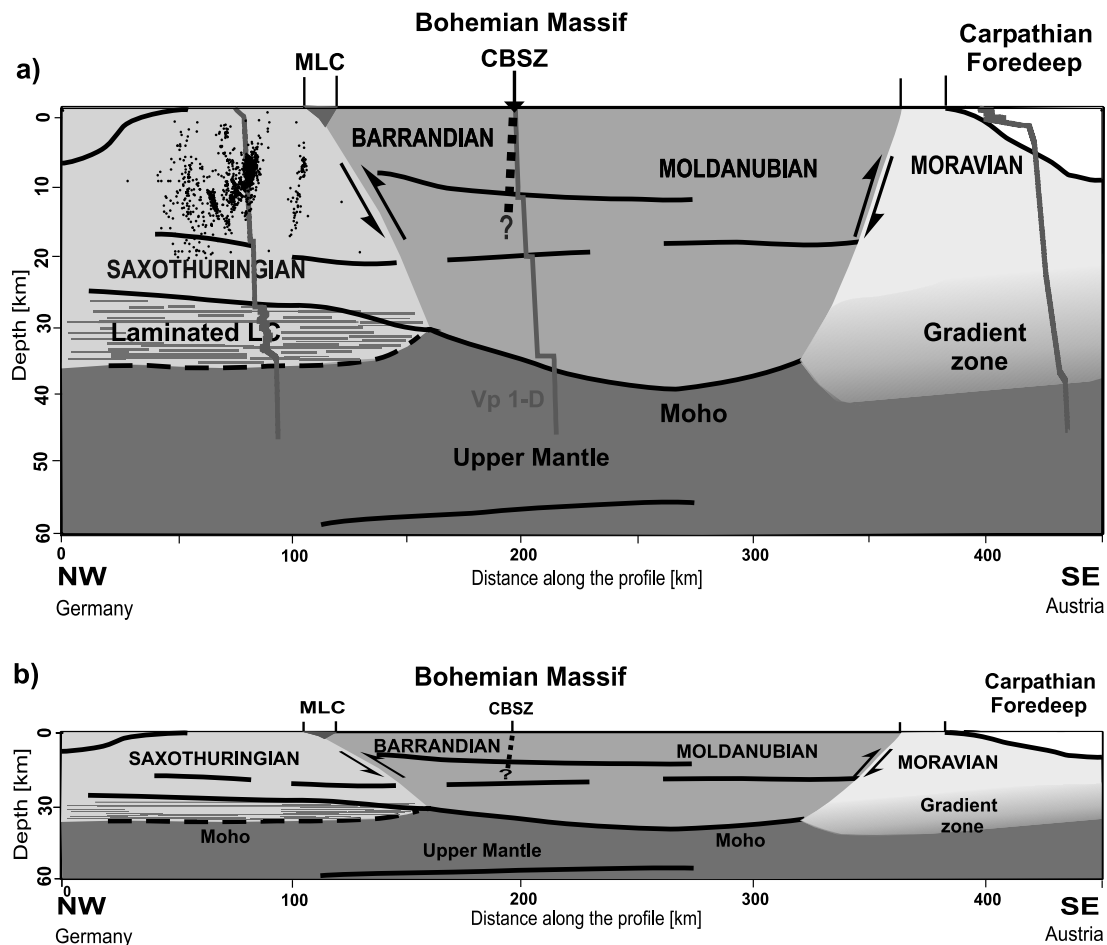


**Figure 13.** Schematic tectonic representation along profile CEL09. Dots show locations of hypocenters of the earthquake swarms in the west Bohemia/Vogtland area. Superimposed are 1-D velocity characteristics showing differentiation in the lower crust for different parts of the Bohemian Massif (from left): the Saxothuringian with laminated lower crust dipping SE; high-velocity contrast at Moho in the Moldanubian; the Moravian with whole crustal gradient zone. Arrows indicate relative movement along contact zones. MLC, Mariánské Lázně Complex; CBSZ, Central Bohemian Shear Zone. (a) Vertical exaggeration of 1:3. (b) Without vertical exaggeration.

rapidly to  $6.0 \text{ km s}^{-1}$  at a depth of 6 km and correlate on the surface with the Carboniferous flysch of the Teuschnitz syncline (see Figure 1). Considerably lower velocities ( $2.5\text{--}5.5 \text{ km s}^{-1}$ ) occur in the SE part of the profile beyond a distance of 400 km, where the Carpathian Foredeep forms an up to 10 km thick sedimentary complex.

[55] Since the profile CEL09 crosses the seismically active west Bohemian region, Figure 13 shows also locations of hypocenters of the earthquake swarms recorded between 1985 and 1998 overlain on the sketch of the crustal structure. In this projection, only hypocenters with the distance smaller than 20 km from the profile were selected. Comparison with the velocity model shows that the hypocenters are located in the upper and middle crustal layer, the majority occurring in the upper crust. The seismically active region coincides well with the location of the lower velocity ( $5.9 \text{ km/s}$ ) region in the upper crust at distances 50–120 km along the CEL09 model, at 0–12 km depth (see Figure 6). According to Špičák and Horálek [2001] this activity may be caused by emission of fluids released by ongoing

magmatic activity and/or fracturing of the crust. As both phenomena decrease seismic velocities, low  $V_p$  may be due to the same factors that cause the seismic activity of the region. However, the relation of velocity decrease to the seismically active area is still a matter of further investigation.

## 10.2. Middle Crust

[56] In the middle crust two reflectors with a velocity contrast of  $0.2 \text{ km s}^{-1}$  were observed in a depth range of 7–12 km and 17–20 km. The first is confined to the area of the Barrandian and partly Moldanubian units, dipping to the SE. The deeper reflection can be traced with few gaps throughout the whole model, and is the most pronounced at a distance of about 350 km, producing very strong reflections for SP 29140 (Figure 4b). The  $V_p$  velocities in the middle crust are in the range of  $6.15\text{--}6.25 \text{ km s}^{-1}$  and display no horizontal variability, as this part of the model is constrained mainly by the reflections from the interface at a depth of 16–20 km.

### 10.3. Lower Crust

[57] In the deeper parts, three different types of lower crust and uppermost mantle can be distinguished. The central part, corresponding to the Moldanubian unit, is characterized by the wave field with sharp onsets of *PmP* phases and a clear *Pn* phase. The lower crust displays average velocities of  $6.8 \text{ km s}^{-1}$  and a strong velocity contrast at Moho modeled as a first-order discontinuity ( $6.8\text{--}8.1 \text{ km s}^{-1}$ ). The Moho depth reaches 39 km and it is the deepest and the most pronounced Moho within the whole Bohemian Massif. This area also correlates with the area of minimum heat flow value ( $<50 \text{ mW m}^{-2}$ ) [Hurtig *et al.*, 1992] and may represent a part of the relatively cold and strong Moldanubian lithosphere [Babuška and Plomerová, 2000]. The crustal thickness also agrees with previous seismic results [e.g., Beránek and Zátapek, 1981; Bucha and Bližkovský, 1994].

[58] The NW part, in the Saxothuringian and partly beneath the Barrandian to a distance of  $\sim 150 \text{ km}$  along the profile, shows high-amplitude reflections from the top of the lower crust with a long coda suggesting strong reflectivity in this layer. The *Pn* phase is weak but visible. The area is interpreted with a highly reflective layer above the Moho, producing a long coda, which obscures a relatively weak *PmP* phase. There is a strong velocity contrast at the top of this layer ( $0.3 \text{ km s}^{-1}$ ) as compared to the contrast at the Moho. The velocities in the lower crust range from  $6.9$  to  $7.3 \text{ km s}^{-1}$ , and its upper boundary is in the depth range of  $25\text{--}27 \text{ km}$ . Moho is represented by a thin (about  $1 \text{ km}$ ) gradient zone where the velocity increases from  $7.3$  to  $7.9 \text{ km s}^{-1}$  at a depth of  $34\text{--}35 \text{ km}$ . The correlation length of the velocity fluctuations in the lower crust was roughly estimated to be  $300 \text{ m}$ . The lamella thicknesses, reported in Variscan areas by other authors, are, e.g.,  $120 \text{ m}$  in Germany [Sandmeier and Wenzel, 1990] or  $100\text{--}300 \text{ m}$  in Poland [Jensen *et al.*, 1999].

[59] CEL09 results in the NW area can be compared with those determined along the perpendicular wide-angle refraction and reflection profiles GRANU'95 and MVE 90 (see Figure 1). The GRANU'95 experiment indicate a velocity increase from  $6.5 \text{ km s}^{-1}$  in the middle crust to an average value of  $7.0 \text{ km s}^{-1}$  at a depth of  $24 \text{ km}$  interpreted as the top of the lower crust [Enderle *et al.*, 1998]. The MVE 90 shows a highly reflective layer in this area at  $8\text{--}10 \text{ s}$  of two-way travel time corresponding to the depth range of  $24\text{--}32 \text{ km}$  [DEKORP Research Group, 1994], which may be viewed as the laminated lower crust found in several Variscan areas. Average  $V_p$  velocities in the lower crust and upper mantle along CEL09 ( $7.1$  and  $7.9 \text{ km s}^{-1}$ , respectively) are consistent with the velocities along GRANU'95 and MVE 90 ( $7.0$  and  $7.9\text{--}8.1 \text{ km s}^{-1}$ , respectively). However, CEL09 crustal thickness is a little larger than in case of GRANU'95 and MVE 90 ( $30$  and  $33 \text{ km}$ ).

[60] According to Enderle *et al.* [1998], elevated lower crustal velocities seem to be characteristic for the Saxothuringian unit. The change of the lower crustal velocities at a distance of  $\sim 150 \text{ km}$  along the CEL09 profile may mark the SE extent of the Saxothuringian lower crust (Figure 13). It correlates with the interpretation of the 9HR [Tomek *et al.*, 1997] and DEKORP 4 profiles [Vollbrecht *et al.*, 1989] where the contact between the Saxothuringian and the units

in the SE is interpreted as a SE dipping overthrust, reaching the base of the crust about  $50\text{--}80 \text{ km}$  to the SE of the contact zone at the surface.

[61] Such a highly reflective lower crust is a phenomenon frequently observed in Caledonian and Variscan areas. It was also found along the deep reflection profiles crossing CEL09 in the Saxothuringian: the MVE 90 and locally 9HR. The most common explanations assume that bands of reflections result from densely spaced layering, produced by igneous intrusions of mafic melt from the upper mantle, subhorizontal ductile shear zones, or layers with higher fluid content [Warner, 1990]. Here, the explanation involving the presence of fluids in the lower crust is not likely, as the *S* wave reflections from the lower crust display very much the same characteristics as the *P* wave in terms of the length of the coda and amplitudes relative to the Moho reflection. Therefore we suggest that lower crustal reflectivity may be caused by mafic intrusions, possibly stretched and arranged horizontally during postorogenic extension.

[62] The SE end of the profile shows strong first arrivals and high reflectivity in the whole crust without any strong intracrustal reflections and with missing *PmP* phase. The overall ringing character of the data and a long coda after the first arrivals is explained by the high reflectivity caused by the small-scale velocity fluctuations in the thick sedimentary sequences of the Carpathian Foredeep. On the basis of the travel time and amplitude character of the data, the lower and middle crust of the Cadomian basement seems to form a thick gradient zone starting at a distance of some  $330 \text{ km}$  along the profile, with velocities of  $6.8\text{--}7.8 \text{ km s}^{-1}$  ranging in a depth of  $23\text{--}40 \text{ km}$ . Such a velocity structure is quite unusual for a relatively old Cadomian unit and its origin is difficult to interpret. It may represent gradual changes of the lower crustal composition, with the percentage of mafic/ultramafic material increasing with depth. Alternative explanation may involve a change in metamorphic grade with an incomplete phase transition of mafic (gabbroic) rocks from amphibolite to eclogite facies. This process is likely to occur continuously over a wide range of pressure, producing a gradual increase of seismic velocities with depth [Furlong and Fountain, 1986]. Hurich *et al.* [2001], studying properties of rock samples of eclogite facies, report velocities and densities for HP granulites in the range of  $7.0\text{--}7.7 \text{ km s}^{-1}$  and  $3.05\text{--}3.3 \text{ g cm}^{-3}$ , respectively, depending on the metamorphic grade. Complete eclogitization is unlikely, as it would result in too high densities ( $3.3\text{--}3.5 \text{ g cm}^{-3}$ ) compared to the model.

[63] During previous investigations, the Moho depth in the SE was not resolved [Beránek and Zátapek, 1981], or was approximated by a discontinuity at a depth of  $32\text{--}35 \text{ km}$  [Bucha and Bližkovský, 1994]. We do not see any evidence for a discontinuity, but our model is consistent with these results, because the overall seismic travel time or gravity effect of the gradient layer will be similar to the effect of a discontinuity located at the center of the layer, given the same average velocity.

### 10.4. Mantle

[64] The local mantle reflector at a depth of  $55\text{--}58 \text{ km}$  in the central part of the Bohemian Massif (distance  $115\text{--}265 \text{ km}$ ) dips slightly to the NW. Its position corresponds to the mantle reflector located on the 9HR profile [Tomek *et al.*

al., 1997] in the cross section with CEL09. Geologically it can be viewed either as a first-order discontinuity or a shear zone with properties different from the neighboring mantle.

## 11. Summary and Conclusions

[65] Seismic data of high quality for interpretation of both the  $P$  and  $S$  wave velocity structure was acquired during the CELEBRATION 2000 experiment along a 450 km long, NW-SE striking profile across the Bohemian Massif. The data have been interpreted by seismic tomography inversion of the travel times of first arrival  $P$  waves, by two-dimensional ray-tracing of travel times of first and later arrivals of  $P$  and  $S$  waves, as well as by calculation of two dimensional synthetic seismograms for the  $P$  wave arrivals. Additional constraint on the crustal structure was given by gravity modeling. Our effort to model these data provides us with the conclusions that are summarized in the tectonic sketch in Figure 13.

[66] The presented crustal model across the Bohemian Massif supplements previous results of geophysical investigations and provides new important information about the structure of the Bohemian Massif, particularly about lower crustal properties and the character of the crust-mantle transition. It helps to verify hypotheses concerning the tectonic evolution of the area during the Paleozoic. Previous wide-angle seismic data provided only generalized information about the velocity distribution (mainly in the upper crust) and about crustal thickness, using methods of kinematic modeling. Our research supplements the kinematic modeling with analysis of the amplitude and character of the seismic wave field and thus gives better insight into the properties of the crust and upper mantle. The boundaries of the main crustal blocks of the Bohemian Massif (Saxothuringian, Barrandian, Moldanubian, Moravian) were previously traced on the surface, based predominantly on the available geological data, whereas the locations of their contact zones at depth were only partially constrained. Our results show differentiation of the structure not only in the upper crustal parts, but mainly at lower crust and upper mantle level, which gives some indications for tracing of crust-forming processes during the Variscan orogeny.

[67] Seismic reflection data along profile 9HR indicated that the Saxothuringian has been underthrust beneath the Barrandian/Moldanubian along a SE dipping thrust zone. The new CEL09 model supports these results and provides additional information for locating the Saxothuringian/Barrandian contact at the lower crustal level. Its location is inferred from the differences between high-velocity, strongly reflective lower crust, which we attribute to the Saxothuringian unit, and moderate-velocity unreflective lower crust and sharp Moho characteristics for the Barrandian/Moldanubian unit. The latter is connected with the crustal thickening of the crystalline segment, the Moldanubian, characterized by the deepest and the most pronounced Moho within the whole Bohemian Massif.

[68] The deep structure of the Moravian unit and its contact with the Moldanubian were, up to now, not constrained by any wide-angle or reflection seismic data. New CELEBRATION 2000 data suggest a peculiar lower crustal/upper mantle structure beneath this region, where a thick crust-mantle transition zone occurs. We postulate that it may

be a characteristic feature of the Moravian unit, and that the western termination of this transition zone may delimit the NW extent of the Moravian lower crust, reaching  $\sim 40$  km farther to the NW than the Moldanubian thrust on the surface. The contact of the above units would form a NW dipping whole crustal zone with the dip of  $45^\circ$  and may represent underthrusting of the Moravian beneath the Moldanubian during the Variscan collision.

[69] **Acknowledgments.** The CELEBRATION 2000 project was supported by the Ministry of Environment of the Czech Republic (VaV 630/00/2), by the Polish State Committee for Scientific Research, Ministry of the Environment of Poland, the Polish Oil and Gas Company, and the Association for Deep Geological Investigations in Poland (ADGIP). The other sponsors were the Geological Survey and the Academy of Sciences of Slovakia, the Eötvös Loránd Geophysical Institute in Hungary, Austrian Academy of Sciences, and the U.S. National Science Foundation (NSF). Seismic stations were provided by the University of Texas at El Paso, IRIS/PASSCAL consortium, and GeoForschungsZentrum Potsdam, Germany. Special thanks are due to Hans Thybo of University of Copenhagen for providing assistance with the reflectivity modeling. The authors also thank Václav Vavryčuk, Ivan Pšenčík, Vladislav Babuška, and anonymous reviewers for reading the manuscript and their valuable comments. Final thanks go to Jozef Vozár, Karoly Posgay, Zoltán Hajnal, and Oguz Selvi for cooperation during the experiment.

## References

- Aki, K., and P. G. Richards (1980), *Quantitative Seismology, Theory and Methods*, W. H. Freeman, New York.
- Babuška, V., and J. Plomerová (2000), Saxothuringian-Moldanubian suture and predisposition of seismicity in the western Bohemian Massif, *Stud. Geophys. Geod.*, *44*, 292–306.
- Beránek, B., and A. Zátocpek (1981), Earth's crust structure in Czechoslovakia and central Europe by methods of explosion seismology, in *Geophysical Synthesis in Czechoslovakia*, edited by A. Zátocpek, pp. 253–264, Veda, Bratislava, Slovakia.
- Beránek, B., and M. Zoumková (1977), Investigations of the Earth's crust in Czechoslovakia using industrial blasting, *Stud. Geophys. Geod.*, *21*, 273–280.
- Bucha, V., and M. Bližkovský (Eds.) (1994), *Crustal Structure of the Bohemian Massif and the West Carpathians*, Academia Praha, Prague, Czech Republic.
- Červený, V., and I. Pšenčík (1984), SEIS83—Numerical modelling of seismic wave fields in 2-D laterally varying layered structures by the ray method, in *Documentation of Earthquake Algorithms*, edited by E. R. Engdál, *Rep. SE-35*, pp. 36–40, World Data Cent. A for Solid Earth Geophys., Boulder, Colo.
- Christensen, N. I. (1996), Poisson's ratio and crustal seismology, *J. Geophys. Res.*, *101*, 3129–3156.
- Christensen, N. I., and W. D. Mooney (1995), Seismic velocity structure and composition of the continental crust: A global view, *J. Geophys. Res.*, *100*, 9761–9788.
- Czuba, W., M. Grad, U. Luosto, G. Motuza, V. Nasedkin, and POLONAISE P5 Working Group (2002), Uppercrustal seismic structure of the Mazury complex and Mazowsze massif within East European Craton in NE Poland, *Tectonophysics*, *360*, 115–128.
- Dallmeyer, D., W. Franke, and K. Weber (1994), *Pre-Permian Geology of Central and Eastern Europe*, Springer, New York.
- DEKORP Research Group (1988), Results of the DEKORP 4/KTB Oberpfalz deep seismic reflection investigations, *J. Geophys.*, *62*, 69–101.
- DEKORP Research Group (1994), The deep reflection seismic profiles DEKORP 3/MVE-90, *Z. Geol. Wiss.*, *22*(6), 623–824.
- Enderle, U., K. Schuster, C. Prodehl, A. Schultze, and J. Briebach (1998), The refraction seismic experiment GRANU'95 in the Saxothuringian belt, southeastern Germany, *Geophys. J. Int.*, *133*, 245–259.
- Finger, F., and H.-P. Steyrer (1995), A tectonic model for the eastern Variscides: Indications from a chemical study of amphibolites in the southeastern Bohemian Massif, *Geol. Carpathica*, *46*(3), 137–150.
- Fischer, T., and J. Horálek (2003), Space-time distribution of earthquake swarms in the principal focal zone of the NW Bohemia/Vogtland seismoactive region: Period 1985–2001, *J. Geodyn.*, *35*, 125–144.
- Franke, W., V. Haak, O. Oncken, and D. Tanner (Eds.) (2000), *Orogenic Processes: Quantification and Modelling in the Variscan Belt*, *Geol. Soc. Spec. Publ.*, *179*, 464 pp.
- Fuchs, K., and G. Müller (1971), Computation of synthetic seismograms with the reflectivity method and comparison with observations, *Geophys. J. R. Astron. Soc.*, *23*, 417–433.

- Furlong, K. P., and D. M. Fountain (1986), Continental crustal underplating: Thermal considerations and seismic-petrologic consequences, *J. Geophys. Res.*, *91*, 8285–8294.
- Giese, P. (1976), Results of the generalized interpretation of the deep-seismic sounding data, in *Explosion Seismology in Central Europe*, edited by P. Giese, C. Prodehl, and A. Stein, pp. 201–214, Springer, New York.
- Grad, M., et al. (2003), Crustal structure of the Trans-European suture zone region along POLONAISE'97 seismic profile P4, *J. Geophys. Res.*, *108*(B11), 2541, doi:10.1029/2003JB002426.
- Guterch, A., et al. (2003), CELEBRATION 2000 Seismic Experiment, *Stud. Geophys. Geod.*, *47*, 659–670.
- Hole, J. A. (1992), Non-linear high-resolution three-dimensional seismic travel time tomography, *J. Geophys. Res.*, *97*, 6553–6562.
- Horálek, J., A. Boušková, F. Hampl, and T. Fischer (1996), Seismic regime of the west-Bohemian earthquake swarm region: Preliminary results, *Stud. Geophys. Geod.*, *40*, 398–412.
- Humphreys, E., and R. W. Clayton (1988), Adaptation of backprojection tomography to seismic travel time problems, *J. Geophys. Res.*, *93*, 1073–1085.
- Hurich, C. A., S. J. Deemer, A. Indares, and M. Salisbury (2001), Compositional and metamorphic controls on velocity and reflectivity in the continental crust: An example from the Grenville Province of eastern Québec, *J. Geophys. Res.*, *106*, 665–682.
- Hurtig, E., V. Čermák, R. Haenel, and V. I. Zui (Eds.) (1992), *Geothermal Atlas of Europe*, set of 36 maps and explanatory note, 156 pp., Hermann Haack Verlagsgesellschaft, Geogr.-Kartogr. Anstalt, Gotha, Germany.
- Jensen, S. L., T. Janik, H. Thybo, and POLONAISE Working Group (1999), Seismic structure of the Palaeozoic Platform along POLONAISE'97 profile P1 in northwestern Poland, *Tectonophysics*, *314*, 123–144.
- Málek, J., M. Brož, T. Fischer, J. Horálek, P. Hrubcová, J. Janský, O. Novotný, and B. Růžek (2001), Seismic measurements along short profiles in western Bohemia during the CELEBRATION 2000 experiment, *Acta Mont., Ser. A*, *18*(121), 15–28.
- Masson, F., B. Jacob, C. Prodehl, P. Readman, P. Shannon, A. Schulze, and U. Enderle (1998), A wide-angle seismic traverse through the Variscan of SW Ireland, *Geophys. J. Int.*, *134*, 689–705.
- Matte, P. (1991), Accretionary history and crustal evolution of the Variscan belt in western Europe, *Tectonophysics*, *196*, 309–337.
- Matte, P. (2001), The Variscan collage and orogeny (480–290 Ma) and the tectonic definition of the Armorica microplate: A review, *Terra Nova*, *13*, 122–128.
- Matte, P., H. Maluski, P. Rajlich, and W. Franke (1990), Terrane boundaries in the Bohemian Massif: Result of large-scale Variscan shearing, *Tectonophysics*, *177*, 151–170.
- Meissner, R., and T. Wever (1986), Nature and development of the crust according to deep reflection data from the German Variscides, in *Reflection Seismology: A Global Perspective*, *Geodyn. Ser.*, vol. 13, edited by M. Barazangi and L. Brown, pp. 31–42, AGU, Washington, D. C.
- Pitra, P., J. P. Burg, and M. Guiraud (1999), Late Variscan strike-slip tectonics between the Tepla-Barrandian and Moldanubian terranes (Czech Bohemian Massif): Petrostructural evidence, *J. Geol. Soc. London*, *156*, 1003–1020.
- Plomerová, J., V. Babuška, and L. Ruprechtová (1984), Velocities of seismic waves propagating through the Bohemian Massif from foci in Poland, *Stud. Geophys. Geod.*, *28*, 56–66.
- Prodehl, C., S. Mueller, and V. Haak (1995), The European Cenozoic Rift System, in *Continental Rifts: Evolution, Structure, Tectonics*, *Dev. Geotectonics*, vol. 25, edited by K. H. Olsen, pp. 133–212, Elsevier, New York.
- Pros, Z., T. Lokajčiek, R. Píkrýl, A. Špičák, V. Vajdová, and K. Klíma (1998), Elastic parameters of West Bohemian granites under hydrostatic pressure, *Pure Appl. Geophys.*, *151*(2-4), 631–646.
- Růžek, B., V. Vavryčuk, P. Hrubcová, J. Zedník, and CELEBRATION Working Group (2003), Crustal anisotropy in the Bohemian Massif, Czech Republic: Observations based on Central European Lithospheric Experiment Based on Refraction (CELEBRATION) 2000, *J. Geophys. Res.*, *108*(B8), 2392, doi:10.1029/2002JB002242.
- Sandmeier, K.-J., and F. Wenzel (1990), Lower crustal petrology from wide-angle P- and S-wave measurements in the Black Forest, *Tectonophysics*, *173*, 495–505.
- Schulmann, K., J. Plomerová, V. Babuška, and O. Lexa (2002), A kinematic model of the structural development of the Moldanubian root during the Variscan orogeny based on correlation of crustal and mantle lithosphere fabrics, *Geolines*, *14*, 82–84.
- Špičák, A., and J. Horálek (2001), Possible role of fluids in the process of earthquake swarm generation in the West Bohemia/Vogtland seismoactive region, *Tectonophysics*, *336*, 151–162.
- Šroda, P., and POLONAISE Profile P3 Working Group (1999), P- and S-wave velocity model of the southwestern edge of the Precambrian East European craton; POLONAISE'97, profile P3, *Tectonophysics*, *314*, 175–192.
- Švancara, J., and M. Chlupáčová (1997), Density model of geological structure along profile 9HR, *J. Geol. Sci. Prague*, *47*, 32–36.
- Thybo, H., and G. Schönharting (1991), Geophysical evidence for early Permian igneous activity in a transtensional environment, Denmark, *Tectonophysics*, *189*, 193–208.
- Thybo, H., et al. (2003), Upper lithospheric seismic velocity structure across the Pripyat Trough and the Ukrainian Shield along the EURO-BRIDGE'97 profile, *Tectonophysics*, *371*, 41–79.
- Tomek, C., V. Dvořáková, and S. Vrána (1997), Geological interpretation of the 9HR and 503 M seismic profiles in western Bohemia, *J. Geol. Sci. Prague*, *47*, 43–51.
- Vavryčuk, V., P. Hrubcová, M. Brož, J. Málek, and ALP 2002 Working Group (2004), Azimuthal variation of P<sub>g</sub> velocity in the Moldanubian, Czech Republic: Observations based on a multi-azimuthal common-shot experiment, *Tectonophysics*, *387*, 189–203, doi:10.1016/j.tecto.2004.06.015.
- Vidale, J. E. (1990), Finite-difference calculation of travel times in three dimensions, *Geophysics*, *55*, 521–526.
- Vollbrecht, A., K. Weber, and J. Schmoll (1989), Structural model for the Saxothuringian-Moldanubian suture in the Variscan basement of the Oberpfalz (northeastern Bavaria, F. R. G.) interpreted from geophysical data, *Tectonophysics*, *157*, 123–133.
- Vrána, S., J. Cháb, and V. Štědrá (1997), Main results of the project, *J. Geol. Sci. Prague*, *47*, 15–23.
- Warner, M. R. (1990), Basalts, water or shear zones in the lower continental crust?, *Tectonophysics*, *173*, 163–173.
- Zeis, S., D. Gajewski, and C. Prodehl (1990), Crustal structure of southern Germany from seismic refraction data, *Tectonophysics*, *176*, 59–86.
- Zelt, C. A. (1994), ZPLOT—An interactive plotting and picking program for seismic data, Bullard Lab., Univ. of Cambridge, Cambridge, U. K.
- Zeyen, H., O. Novak, M. Landes, C. Prodehl, L. Driad, and A. Hirn (1997), Refraction-seismic investigations of the northern Massif Central, *Tectonophysics*, *275*, 99–117.

E. Brueckl, Vienna University of Technology, Gusshausstrasse 27-29, A-1040 Vienna, Austria. (ebrueckl@luna.tuwien.ac.at)

M. Grad, Institute of Geophysics, University of Warsaw, Pasteura 7, PL-02-093 Warsaw, Poland. (mgrad@mimuw.edu.pl)

A. Guterch and P. Šroda, Institute of Geophysics, Polish Academy of Sciences, Ks. Janusza 64, PL-04-152 Warsaw, Poland. (aguterch@igf.edu.pl)

P. Hrubcová and A. Špičák, Geophysical Institute, Academy of Sciences of the Czech Republic, Bočni II/1401, 141 31 Prague 4, Czech Republic. (pavla@ig.cas.cz)

G. R. Keller, Department of Geological Sciences, University of Texas at El Paso, El Paso, TX 79968, USA. (keller@geo.utep.edu)

H. Thybo, Geological Institute, University of Copenhagen, Oster Voldgade 10, DK-1350 Copenhagen, Denmark. (thybo@geol.ku.dk)